

Experimental and Computational Studies of Intracomplex Reactions in Mg^+ (Primary, Secondary Alkylamine) Complexes Induced by Photoexcitation of Mg^+

Haichuan Liu,^[a] Yihua Hu,^[a] Shihe Yang,^{*,[a]} Wenye Guo,^{*,[b]} Xiaoqing Lu,^[b] and Lianming Zhao^[b]

Abstract: We report herein a comprehensive study of photoinduced reactions in complexes of Mg^+ with primary (*n*-propyl- and isopropylamine) and secondary amines (dipropyl- and diisopropylamine) in the spectral range of 230–440 nm. Similar to the methyl- and ethylamine complexes studied previously, N–H bond activation of these complexes is very unfavorable. Instead, the C^α –C, C–N, and C^α –H bond-cleavage photoproducts are observed after photoexcitation of the Mg^+ complexes ($3^2\text{P} \leftarrow 3^2\text{S}$). For Mg^+ (primary amine) complexes, for example, Mg^+ –

$\text{NH}_2\text{CH}_2\text{CH}_2\text{CH}_3$, and Mg^+ – $\text{NH}_2\text{CH}(\text{CH}_3)_2$, the photoproducts resulting from C^α –C rupture prevail after P_z and charge-transfer excitations, whereas the Mg^+ photofragment is predominant upon $\text{P}_{x,y}$ excitation. However, with further *N*-alkyl substitution, as in Mg^+ (secondary amine) complexes, for example, Mg^+ – $\text{NH}(\text{CH}_2\text{CH}_2\text{CH}_3)_2$ and

Mg^+ – $\text{NH}[\text{CH}(\text{CH}_3)_2]_2$, a novel intracomplex C–C coupling photoreaction dominates on $\text{P}_{x,y}$ excitation of Mg^+ , which is believed to arise from Mg^{+*} insertion into the C–N bond. With P_z and charge-transfer excitation, the Mg –R elimination photoproducts, arising from C^α –C bond cleavage, predominate. The energetics and possible mechanisms of the intracomplex photoreactions are analyzed in detail with the help of extensive quantum mechanics calculations.

Keywords: bond activation • laser chemistry • mass spectrometry • metal complexes • photodissociation

Introduction

For the past three decades, considerable effort has been spent investigating the gas-phase reactions of metal ions with organic molecules.^[1–5] Ion cyclotron resonance (ICR), ion-beam techniques, and other mass spectrometric methods have been used to study ion–molecule reactions. These stud-

ies have significantly advanced our knowledge of the reactions between metal ions and organic molecules. Lately, we have studied intracomplex reactions in metal⁺(organic molecule) complexes initiated by the electronic excitation of the metal⁺ species.^[6,7] Here the reaction is designed to start from a well-defined configuration and is triggered by the absorption of a photon by the metal⁺ moiety. As such, the metal⁺ moiety not only provides an effective chromophore with an unpaired electron but also allows the photoreactions to be traced through the positive charge, which can be detected by mass spectrometry with nearly 100 % efficiency.

In a set of recent experiments, we studied the photodissociation of Mg^+ (mono-, dimethylamine)^[7a] [Mg^+ – NH_2CH_3 and Mg^+ – $\text{NH}(\text{CH}_3)_2$] and Mg^+ (di-, triethylamine) [Mg^+ – $\text{NH}(\text{CH}_2\text{CH}_3)_2$ and Mg^+ – $\text{N}(\text{CH}_2\text{CH}_3)_3$].^[7b] It was found that C–H bond activation is the main or exclusive reactive channel in the photodissociation of Mg^+ – NH_2CH_3 and Mg^+ – $\text{NH}(\text{CH}_3)_2$. In contrast, the photoreactions of Mg^+ (di-, triethylamines) are dominated by C–N/C–C bond activation, which results in an intriguing C_3H_7^+ elimination channel. This was explained in terms of steric effects and the ac-

[a] H. Liu, Y. Hu, Prof. S. Yang
Department of Chemistry
The Hong Kong University of Science and Technology
Clear Water Bay, Kowloon, Hong Kong (P. R. China)
Fax: (+852) 2358-1594
E-mail: chsyang@ust.hk

[b] W. Guo, X. Lu, L. Zhao
College of Physical Science and Technology
Chinese University of Petroleum
Dongying, Shandong 257061 (P. R. China)
Fax: (+86) 0546-839-2123
E-mail: wyguo@mail.hdpu.edu.cn

Supporting information for this article is available on the WWW under <http://www.chemurj.org/> or from the author. Calculated structures and energies of some species and reactions.

cessibility of the C–H bonds of the methyl groups. Moreover, photoproducts were observed in the spectral regions of both $3P_{x,y}$ and $3P_z$ for $Mg^+-NH_2CH_3$ and $Mg^+-NH(CH_3)_2$, in contrast to the case of Mg^+ (di-, triethylamine), from which C–H and C–N scission products are formed only in the $3P_{x,y}$ excitation region. Charge-transfer (CT) photodissociation products were observed from Mg^+ (ammonia) and Mg^+ (methylamine), but not from Mg^+ (dimethylamine), Mg^+ (diethylamine), and Mg^+ (triethylamine). It appears that crossing between the initially accessed $3P$ surfaces and CT surfaces plays an important role, and therefore the relative energies of the states in the Franck–Condon region dictate the likelihood of photoinduced CT dissociation.

Although a lot has been learned from our previous photodissociation studies of Mg^+ (amines), some questions remain unanswered. Particularly puzzling is the propensity for C–N and C–C bond activation by Mg^{+*} . This is closely related to the mechanism of the C_3H_7 elimination that occurs in the photoinduced intracomplex C–C coupling reactions in $Mg^+-NH(CH_2CH_3)_2$ and $Mg^+-N(CH_2CH_3)_3$.^[7b] Because the photoinduced intracomplex C–C coupling reactions only take place with secondary and tertiary amines in which the alkyl groups have more than one carbon atom, it is logical to extend the photodissociation study to complexes of secondary amines with longer alkyl chains. To gain an insight into the reactions that follow C–N or C–C bond activation, it would also be interesting to study primary amines with longer alkyl chains, which may shed light on the initial step of the C–C coupling reactions that occur in complexes of secondary and tertiary amines. In this way, a coherent picture of the mechanisms of the photoinduced reactions that occur in this type of complex is expected to emerge. It is also important to identify which bonds in the alkylamines can be activated after photoexcitation of the N-coordinating metal ion, Mg^+ . Towards this end, we have studied the photodissociation of complexes formed between Mg^+ and *n*-propyl-, isopropylamine, dipropyl-, and diisopropylamine. It turns out that these systems reveal more about the photoreaction mechanisms of metal⁺(amine) complexes; state-specific photoreactions have been observed. Extensive quantum mechanics calculations have been performed to assist the interpretation of the photoinduced reactions. In this paper we report the bulk of these experimental and computational results, and, together with previous results,^[7] we present an overview of the current understanding of the mechanisms of the photoreactions of Mg^+ (alkylamine) complexes.

Experimental and Computational Section

Photodissociation experiments: The experimental details for the experiments carried out in this work are the same as those described previously,^[8] and therefore only a very brief description is given here. Mg^+ ions were produced by focusing the second harmonic (532 nm) of a Nd:YAG laser on a ~1 mm diameter spot on a rotating magnesium disk. A pulsed valve was employed to generate propyl- and isopropylamine clusters by supersonic expansion of the vapor of the organic molecules seeded in

helium. The laser-generated species, including Mg^+ , traversed the supersonic jet stream perpendicularly, forming a series of Mg^+-S_n species (*S* = propyl- and isopropylamine). The nascent clusters then traveled 14 cm to the extraction region of the reflectron time-of-flight spectrometer (RTOFMS). For the photodissociation experiments, a desired peak was selected with a mass gate, and irradiated with a photolysis dye laser beam. The parent and nascent daughter cations were detected with a microchannel plate (MCP) detector. The photolysis laser fluence was kept low ($<1 \text{ mJ cm}^{-2}$) to avoid multiphoton processes. By monitoring the photofragment ion intensities as the dye laser wavelength was scanned, channel-resolved spectra of all the observed photofragment ions were obtained. The action spectra were normalized by the parent-ion intensities and the laser fluences.

Computational details: Quantum-mechanics calculations were performed with the Gaussian 03 program.^[9] The observed photoreactions, although initiated by electronic excitation, were assumed to occur on the ground-state surface after internal charge transfer. All species were calculated using density functional theory with the B3LYP method^[10] using the 6-31+G** basis set. Each stationary point was characterized by vibrational frequency analysis (minimum with zero; transition state with one imaginary frequency). To confirm the transition-state structures for some key reaction pathways, intrinsic reaction coordinate (IRC) calculations were used to follow the reaction pathways. All the relative energies are reported with zero-point energy (ZPE) corrections. The ZPE scaling factor was selected as 0.989.^[11] Note that problems in dealing with radical cations often arise with the use of the DFT/B3LYP method.^[12,13] Higher-level calculations such as CCSD(T) would be desirable to obtain more accurate results, however, we did not resort to these more costly methods because the level of our calculations is sufficient to understand the reaction pathways based on the experimentally observed products. As a test case, we calculated the bond dissociation energies (BDEs) of Mg^+ (propylamine) ($50.3 \text{ kcal mol}^{-1}$) and Mg^+ (isopropylamine) ($50.5 \text{ kcal mol}^{-1}$) at the MP2/6-31G(d) level of theory. These BDEs are fairly consistent with the values calculated at the B3LYP/6-31+G** level of theory (both are $\sim 43.8 \text{ kcal mol}^{-1}$).

The vertical excitation energies and corresponding oscillator strengths of the Mg^+ (propylamine) complexes were calculated by the TD-B3LYP/6-311++G** method using the B3LYP/6-31+G**-derived geometries.

Results and Discussion

Photodissociation action spectra: Figure 1 displays the photodissociation action spectra of $Mg^+-NH_2CH_2CH_2CH_3$, $Mg^+-NH_2CH(CH_3)_2$, and $Mg^+-NH[CH(CH_3)_2]_2$ over the wavelength range of 230–440 nm. The action spectra (Figure 1a–c) are very similar to each other with two pronounced bands: one is on the red side (centered at $\sim 370 \text{ nm}$) and the other is on the blue side (centered at $\sim 260 \text{ nm}$) of the $Mg^+ 3^2P \leftarrow 3^2S$ atomic transition. However, the high-energy peak of $Mg^+-NH[CH(CH_3)_2]_2$ (Figure 1c) is somewhat more blue-shifted than those of $Mg^+-NH_2CH_2CH_2CH_3$ and $Mg^+-NH_2CH(CH_3)_2$ (Figure 1a and b). This indicates that the interaction of $NH[CH(CH_3)_2]_2$ with the p_o orbital of Mg^+ is stronger, which is expected because there are two isopropyl groups connected to the nitrogen atom. Furthermore, the red-shifted band of $Mg^+-N[CH(CH_3)_2]_2$ exhibits only a broad feature (Figure 1c), whereas two peaks can be seen in this region for $Mg^+-NH_2CH_2CH_2CH_3$ and $Mg^+-NH_2CH(CH_3)_2$ (Figure 1a and 1b). Most likely, secondary amine complexes have many more degrees of freedom and thus the p_π -derived states have broader action spectra, which eventually overlap. In addition, the secondary amine com-

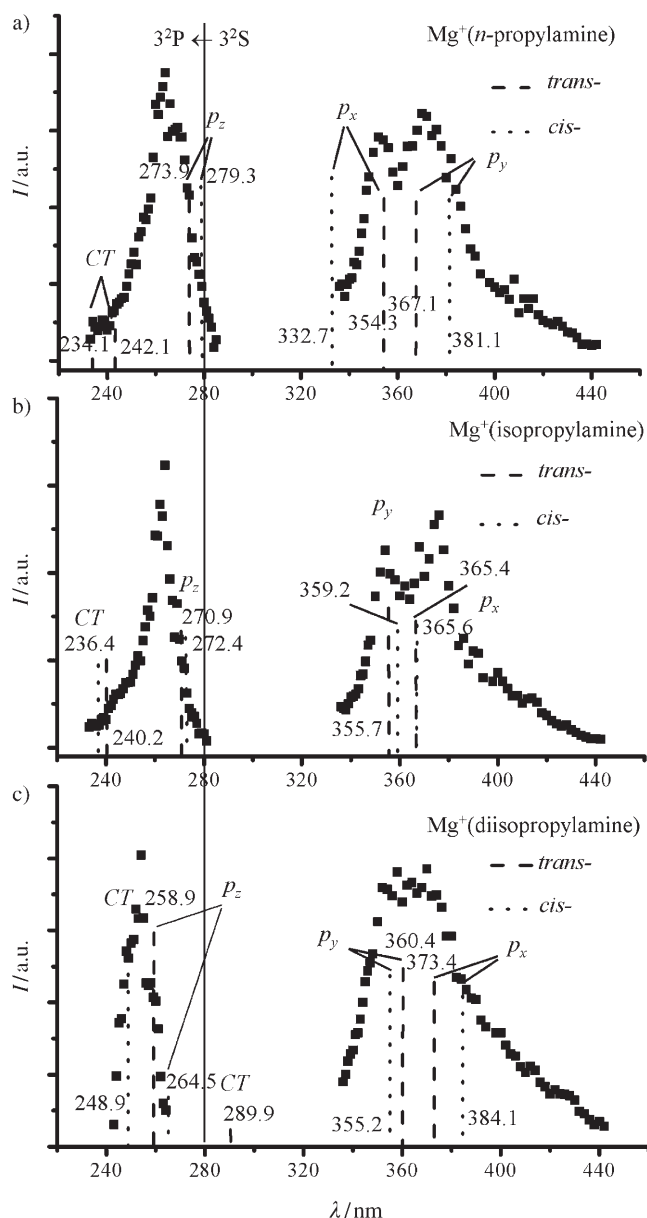


Figure 1. Action spectra of a) $\text{Mg}^+(\textit{n}\text{-propylamine})$, b) $\text{Mg}^+(\textit{isopropylamine})$, and c) $\text{Mg}^+(\textit{diisopropylamine})$. The solid line indicates the atomic transition of Mg^+ ($3^2\text{P} \leftarrow 3^2\text{S}$), while the dashed and dotted lines show the absorption spectra (excitation energies and oscillator strengths) calculated at the TD-B3LYP/6-311++G** level of theory. I = relative intensity.

plexes have more isomers and this further contributes to the overlapping in the spectra of the p_π -derived states.

To understand the action spectra, we performed a series of quantum mechanics calculations. First, ground-state structures were optimized at the B3LYP/6-31+G** level of theory. *cis* and *trans* structures, when existent, were calculated for comparison. Figure 2 shows the geometries obtained along with the geometrical parameters of the parent complexes $\text{Mg}^+\text{-NH}_2\text{CH}_2\text{CH}_2\text{CH}_3$ (**1**), $\text{Mg}^+\text{-NH}_2\text{CH}(\text{CH}_3)_2$ (**2**), $\text{Mg}^+\text{-NH}(\text{CH}_2\text{CH}_2\text{CH}_3)_2$ (**3**), and $\text{Mg}^+\text{-NH}[\text{CH}(\text{CH}_3)_2]_2$ (**4**). Parameters for the optimized geometries of the free

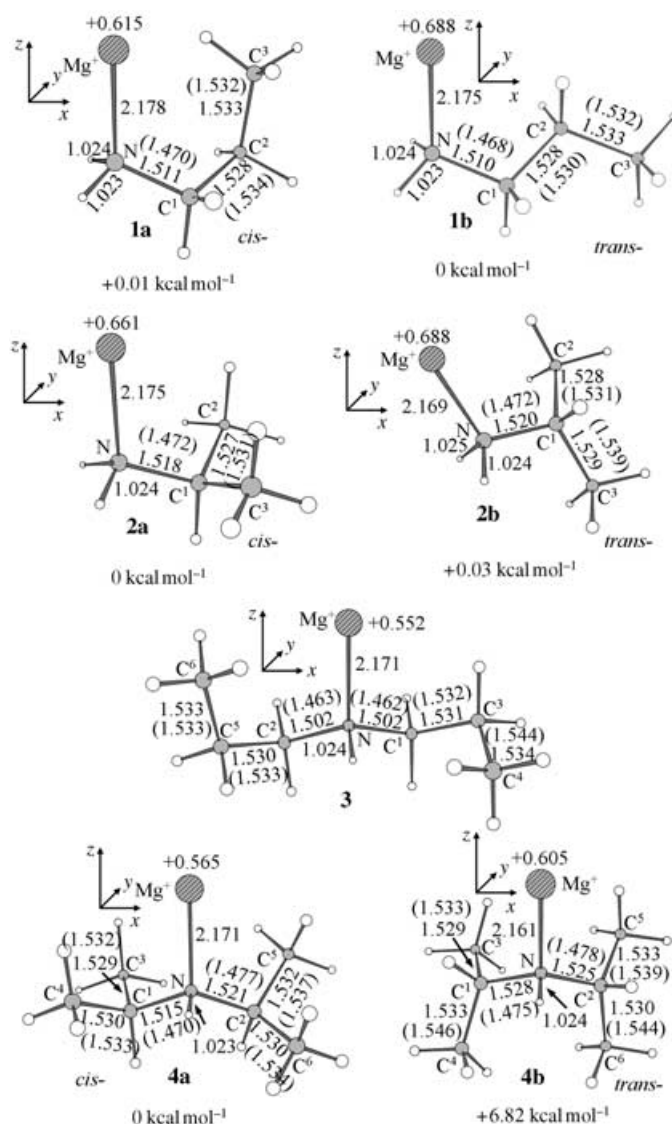


Figure 2. Possible ground-state structures of the complexes $\text{Mg}^+(\textit{n}\text{-propylamine})$ (**1**), $\text{Mg}^+(\textit{isopropylamine})$ (**2**), $\text{Mg}^+(\textit{dipropylamine})$ (**3**), and $\text{Mg}^+(\textit{diisopropylamine})$ (**4**) optimized at the B3LYP/6-31+G** level of theory.

molecules are also given in parentheses for comparison. For the primary amines, it can be seen that the stabilities of the *cis* (**1a**, **2a**) and *trans* (**1b**, **2b**) structures of **1** and **2** are nearly the same, indicating the coexistence of the isomers in the gas phase. However, for the secondary amines, the *cis* structure (**4a**) of $\text{Mg}^+\text{-NH}[\text{CH}(\text{CH}_3)_2]_2$ is 6.82 kcal mol⁻¹ more stable than the *trans* conformer (**4b**). Owing to its relatively long alkyl chains, $\text{Mg}^+\text{-NH}(\text{CH}_2\text{CH}_2\text{CH}_3)_2$ (**3**) is expected to have more stereoisomers than **1**, **2**, and **4**. We have calculated only one conformer of **3** (see Figure 2), which actually has a *cis*-like form similar to that of **1a**. The BDEs of both the *trans* and *cis* forms of $\text{Mg}^+(\textit{n}\text{-propylamine})$ and $\text{Mg}^+(\textit{isopropylamine})$ are very similar (~44 kcal mol⁻¹). *N*-Alkyl substitution increases the BDE

slightly, being $47.0 \text{ kcal mol}^{-1}$ for $\text{Mg}^+-\text{HN}(\text{CH}_2\text{CH}_2\text{CH}_3)_2$ and $47.3 \text{ kcal mol}^{-1}$ for $\text{Mg}^+-\text{HN}[\text{CH}(\text{CH}_3)_2]_2$.

On the basis of our calculations, the complexes of **1–4** are all characterized by the linkage of Mg^+ to the nitrogen atoms of the amine molecules. The overall symmetries of **2a** and **4a,b** are nearly C_s with the symmetry plane defined by the $\text{Mg}-\text{N}-\text{C}^\alpha$ and $\text{Mg}-\text{N}-\text{H}$ planes for **2a** and **4a,b**, respectively (see Figure 2). Other complexes (**1a**, **1b**, **2b**, and **3**) have no symmetry elements other than C_1 . Relative to the structures of the free amines, the $\text{N}-\text{C}$ bonds are lengthened by $\sim 3.0\%$ by complex formation. In accord with the BDE changes mentioned above, the Mg^+-N bonds are shortened further in going from the primary to secondary amine complexes.

By using the optimized ground-state geometries described above, the absorption spectra of Mg^+ (propyl-, isopropyl-, and diisopropylamine) were calculated at the TD-B3LYP/6-311++G** level of theory and are depicted in Figure 1 by dashed lines for the *trans* complexes and dotted lines for the *cis* complexes. The calculated absorption spectra of the *trans* forms are not significantly different from those of the corresponding *cis* forms (Figure 1). Perhaps the main exception is the spectrum of Mg^+ (propylamine) in the red region (Figure 1a), which suggests that the linear alkyl chain in *n*-propylamine has different steric effects in the excited states. On the red side of the Mg^+ atomic transition, the two spectral lines are calculated to correspond to the $3s \rightarrow 3p_{xy}$ transition, while the $3s \rightarrow 3p_z$ and $n_N \rightarrow 3s$ (β -spin) excitations are located on the blue side. In the two 3^2P_{xy} -type excited states of Mg^+ (propyl-, isopropyl-, and diisopropylamine) (see the coordinate designation in Figure 2), the two $3p_{xy}$ orbitals of Mg^+ are perpendicular to the Mg^+-N bond axis, hence the energies are lowered as a result of reduced electron repulsion. While the $3p_y$ orbital of Mg^+ is aligned perpendicularly to the $\text{Mg}-\text{N}-\text{C}$ plane, the $3p_x$ orbital lies in the plane and therefore has a similar symmetry to that of the σ^* -antibonding orbital of the $\text{C}-\text{N}$ bond. The resultant interaction endows the Mg^+-N bond with some covalent character and lowers the energy of the $3P_x$ -type state, giving rise to a further red shift relative to the $3P_y$ -type state. The peak on the blue side of the action spectrum is ascribed to the 2P_z -type excited state and a charge-transfer state (2A in C_1 or $^2A'$ in C_s). In the 2P_z -type state, the occupied $3p_z$ orbital is aligned along the Mg^+-N bond axis, hence raising its energy as a result of the direct repulsion between the $3p_z$ electron and the nitrogen lone-pair electrons. As shown in Figure 1, with the exception of *trans*- Mg^+ (diisopropylamine), CT states ($n_N \rightarrow 3s$) generally lie above the 2P_z -type states for most Mg^+ (propylamine) complexes.

Experimental photodissociation mass spectra: Because of their similarities for the four complexes in our study, only selected photodissociation difference mass spectra ($I_{\text{laser on}} - I_{\text{laser off}}$) of $\text{Mg}^+-\text{NH}_2\text{CH}_2\text{CH}_2\text{CH}_3$ and $\text{Mg}^+-\text{NH}[\text{CH}(\text{CH}_3)_2]_2$ are shown in Figure 3 and Figure 4, respectively. Note that the downward peaks indicate the disappearance of parent complexes, and the upward peaks correspond

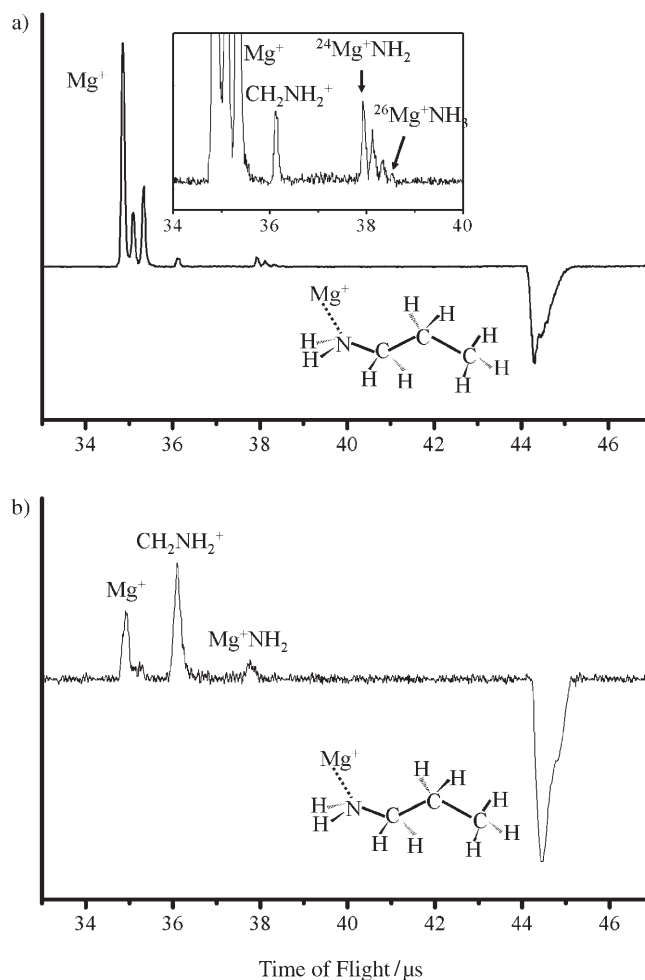


Figure 3. Photodissociation difference mass spectra of Mg^+ (*n*-propylamine) at a) 362 and b) 260 nm. The inset in a) is a close-up view in the time frame of 34–40 μs .

to the appearance of daughter ions. For the sake of comparison, the relative intensities of the photoproducts from the four complexes at different wavelengths are collected in Table 1. In general, the two primary complexes exhibit very similar photodissociation features. At the long wavelength (362 nm, Table 1), the dominant photofragment for both complexes is Mg^+ . However, the photoreaction products CH_2NH_2^+ and $\text{CH}_3\text{CH}^+\text{NH}_2$, which result from $\text{C}^\alpha-\text{C}$ bond rupture, are dominant at the short wavelength (260 nm). Some minor photoproducts are also observed at both long and/or short wavelengths, including Mg^+NH_2 and Mg^+NH_3 , which are clearly generated by $\text{C}-\text{N}$ bond activation. $(\text{CH}_3)_2\text{CNH}_2^+$ is also formed from $\text{Mg}^+-\text{NH}_2\text{CH}(\text{CH}_3)_2$ probably through $\text{C}^\alpha-\text{H}$ bond activation at long wavelengths.

For both secondary complexes, copious photofragments, including Mg^+ , are observed in the long wavelength region (Figure 4 and Table 1), whereas only two photofragments (Mg^+ and $[\text{L}^1-\text{C}_2\text{H}_5]^+$ or $[\text{L}^2-\text{CH}_3]^+$, L^1 =dipropylamine; L^2 =diisopropylamine) are detected at the short wavelength. Four types of photoproducts can be recognized at the long

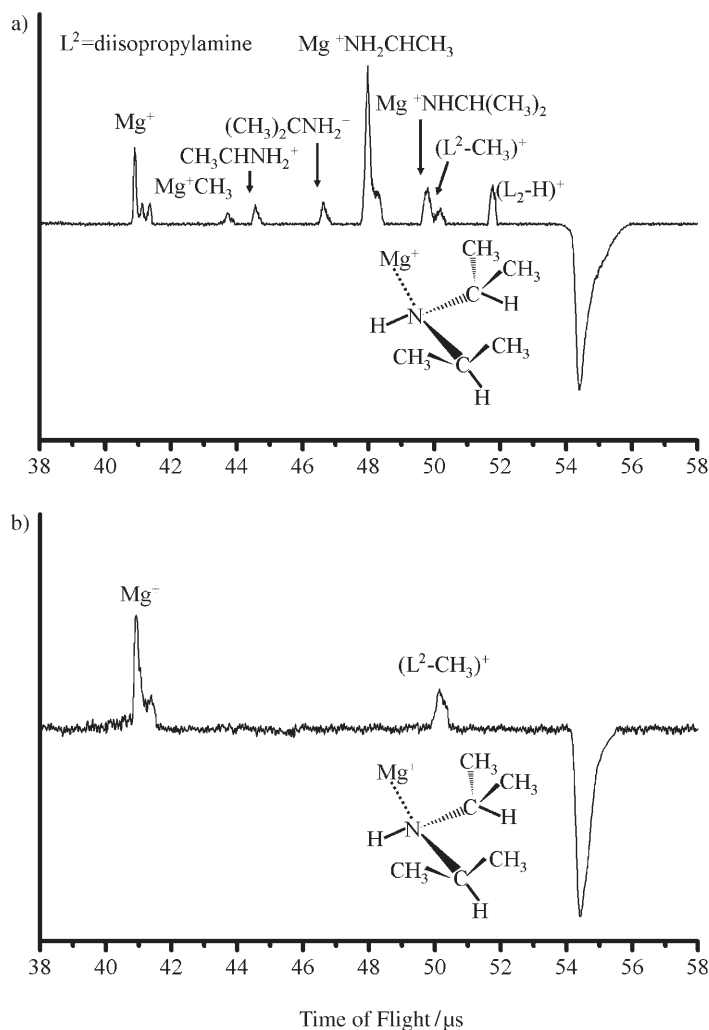


Figure 4. Photodissociation difference mass spectra of $\text{Mg}^+(\text{diisopropylamine})$ at a) 362 and b) 251 nm.

wavelength. The first are (Mg^+, N) -containing photoproducts, for example, $\text{Mg}^+-\text{NC}_2\text{H}_6$ and $\text{Mg}^+-\text{NC}_3\text{H}_8$ for both complexes and Mg^+-NCH_4 for the complex with linear alkyl groups, which result from a dominant photoreaction

channel probably through C–N or C^α –C bond activation followed by intracomplex reactions. Small iminium ions such as CH_2NH_2^+ from $\text{Mg}^+(\text{dipropylamine})$ and $\text{CH}_3\text{CHNH}_2^+$ and $(\text{CH}_3)_2\text{CNH}_2^+$ from $\text{Mg}^+(\text{diisopropylamine})$ constitute the second type of photoproducts, which also come from C–N or C^α –C bond activation and subsequent intracomplex reactions. Among the third type of photoproducts are $[\text{L}-\text{C}_2\text{H}_5]^+$, Mg^+-CH_3 , and $[\text{L}-\text{CH}_3]^+$, which are formed by C^α –C bond activation. Finally, C^α –H bond activation yields photoproducts such as $[\text{L}-\text{H}]^+$.

In the long wavelength range (>330 nm), the major photofragment, Mg^+ , from both primary complexes has a branching fraction of $>80\%$ and is roughly independent of the wavelength. The branching fractions of the minor photoproducts also only change slightly in this region. The branching fractions for the two primary amine complexes, being nearly constant at long wavelengths, are only given in the short wavelength region (Figure 5a and 5b), while those of the $\text{Mg}^+(\text{diisopropylamine})$ complex are presented over the whole spectral region (Figure 5c). As one can see, the branching fractions of Mg^+ and the iminium photoproducts $[\text{CH}_2\text{NH}_2^+]$ from $\text{Mg}^+-\text{NH}_2\text{CH}_2\text{CH}_2\text{CH}_3$ and $\text{CH}_3\text{CHNH}_2^+$ from $\text{Mg}^+-\text{NH}_2\text{CH}(\text{CH}_3)_2$ vary markedly with the wavelength and seem to be anti-correlated. For Mg^+NH_2 , the branching fractions are nearly constant. The situation for $\text{Mg}^+-\text{NH}[\text{CH}(\text{CH}_3)_2]_2$ is somewhat different (Figure 5c). In the long wavelength region, Mg^+ and $[\text{L}^2-\text{H}]^+$ exhibit noteworthy complementary changes in the branching fraction changes, whereas the branching fractions of the main photoproduct $\text{Mg}^+-\text{NH}_2\text{CHCH}_3$ and other minor photoproducts are relatively constant. There are only two photofragments in the short wavelength range: Mg^+ (major) declines with decreasing wavelength accompanied by an increase in $[\text{L}^2-\text{CH}_3]^+$ (minor). The approximately constant branching fractions in the long wavelength region imply that these photoproducts are generated in a common process, whereas the varying branching fractions in the short wavelength region indicate either competition between the two different product channels or that different initial states accessed by optical excitation. For the latter, Mg^+ and $[\text{L}-\text{R}]^+$ are produced by the excitation of the $^2\text{P}_z$ -type and CT states, re-

Table 1. Relative intensities of the photofragments of $\text{Mg}^+(\text{propyl-}, \text{dipropyl-}, \text{isopropyl-}, \text{ and diisopropylamine})$ at selected wavelengths.

| Amine | λ [nm] | Relative intensity [%] | | | | | | | | | | |
|------------------------------------|-------------------|------------------------|--|--|--------------------------------------|--|--|--|--|--|--------------------|--------------------|
| | | Mg ⁺ | ²⁴ Mg ⁺ – NH ₂ | ²⁶ Mg ⁺ – NH ₃ | Mg ⁺ – CH ₃ | CH ₂ NH ₂ ⁺ | CH ₃ CHNH ₂ ⁺ / –(CH ₃) ₂ CNH ₂ ⁺ | Mg ⁺ – NH ₂ CH ₄ | Mg ⁺ – NC ₂ H ₆ ^[a] | Mg ⁺ – NC ₃ H ₈ ^[b] | L–R ^[c] | L–H ^[c] |
| Mg ⁺ (propylamine) | 362 | 91.1 | 4.2 | 0.8 | – | – | – | – | – | – | 3.9 | – |
| | 260 | 33.5 | 15.7 | – | – | – | – | – | – | – | 53.7 | – |
| Mg ⁺ (isopropylamine) | 362 | 84.5 | 8.6 | 1.7 | – | – | – | – | – | – | 2.6 | 2.6 |
| | 260 | 37.1 | 17.7 | – | – | – | – | – | – | – | 45.3 | – |
| Mg ⁺ (dipropylamine) | 370 | 36.4 | – | – | – | 5.1 | – | 30.0 | 7.6 | 5.6 | 9.4 | 5.8 |
| | 245 | 75.8 | – | – | – | – | – | – | – | – | 24.2 | – |
| Mg ⁺ (diisopropylamine) | 362 | 19.6 | – | – | 3.6 | – | 5.6/6.3 | – | 39.7 | 9.8 | 4.8 | 10.5 |
| | 251 | 68.5 | – | – | – | – | – | – | – | – | 31.5 | – |

[a] $\text{Mg}^+-\text{NH}_2\text{CH}_2\text{CH}_2$ and $\text{Mg}^+-\text{NH}_2\text{CHCH}_3$ for $\text{Mg}^+(\text{dipropylamine})$ and $\text{Mg}^+(\text{diisopropylamine})$, respectively. [b] $\text{Mg}^+-\text{NHCH}_2\text{CH}_2\text{CH}_3$ and $\text{Mg}^+-\text{NHCH}(\text{CH}_3)_2$ for $\text{Mg}^+(\text{dipropylamine})$ and $\text{Mg}^+(\text{diisopropylamine})$, respectively. [c] L = amine molecular ion.

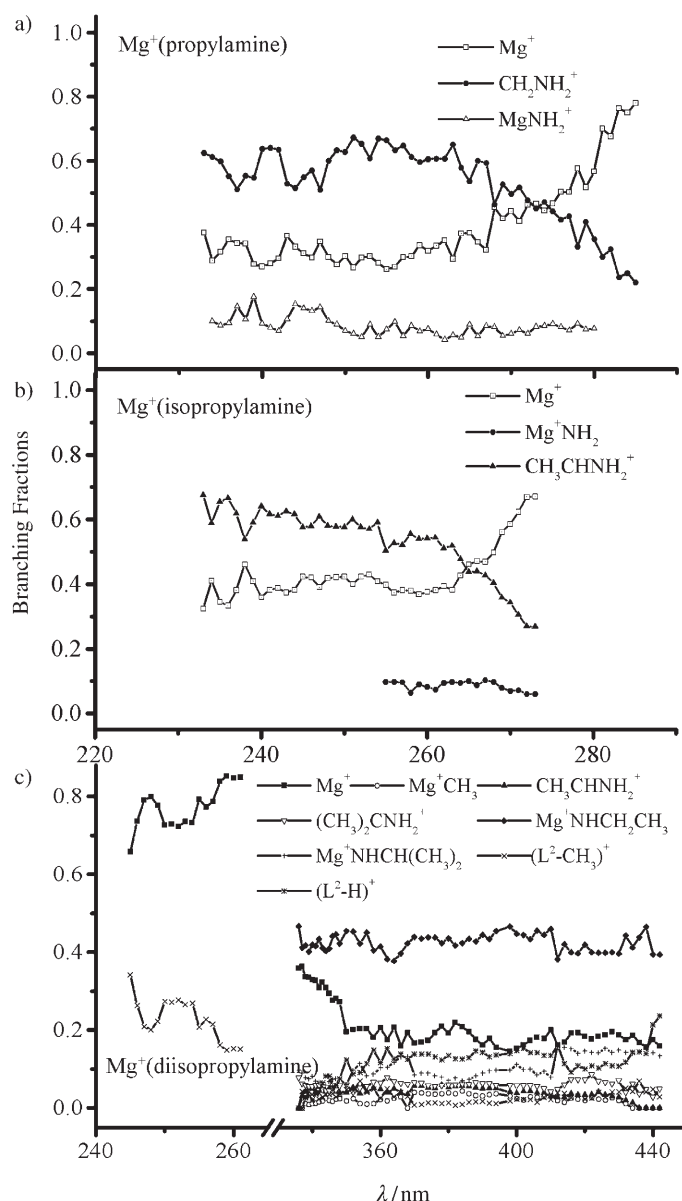
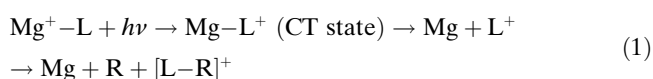


Figure 5. Photofragment branching fractions from a) $\text{Mg}^+(n\text{-propylamine})$, b) $\text{Mg}^+(\text{isopropylamine})$, and c) $\text{Mg}^+(\text{diisopropylamine})$ as a function of the photolysis laser wavelength.

spectively [for CT excitation we refer to the sequence given in Eq. (1)]. This is consistent with the calculated absorption spectra shown in Figure 1.



Intracomplex reactions: The evaporative photofragment Mg^+ is almost always observed in the photodissociation of $\text{Mg}^+(\text{organic molecules})$. In the case of amine complexes, excited-state reaction mechanisms can be ruled out owing to insufficient photon energies as discussed previously.^[6,7] In the $\text{P}_{x,y}$ excitation region both the reactive and the nonreac-

tive photofragments have constant branching fractions and an electronic–vibrational (E–V) quenching mechanism that involves internal conversion from the excited state to the ground state is believed to be operative here. Thus the photoproducts resulting from C–C, C–N, and C–H bond activations most likely arise from nonadiabatic transitions from the initial excited states through curve crossings (or conical intersections) to the ground-state surfaces with vibrational excitations at least in the $\text{P}_{x,y}$ excitation region. The photochemistry in the P_z excitation region is notably different, and may involve the dynamics of the $^2\text{P}_z$ -type and CT states. Below we will discuss the photoreactions of the primary and secondary amine complexes and their possible mechanisms in the $\text{P}_{x,y}$ excitation region.

Calculated geometries and energetics of photoproducts: Table 2 summarizes the key results of our calculations on the photofragments of iminium cations (**P-1** to **P-6**) and (Mg^+, N)-containing photoproducts (**P-7** to **P-10**) derived from complexes **1–4**. The photodissociation energies are tabulated in Table 3. It is found that the C=N bond in the iminium photoproducts is lengthened with methyl substitution at the α -carbon atom and is accompanied by a reduction in the ionization energy (IE) (see Table 2), for example,

Table 2. Summary of the calculations on some of the photoproducts.

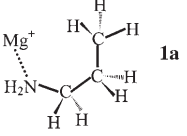
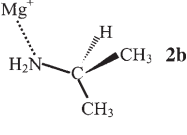
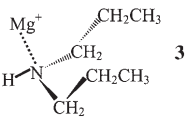
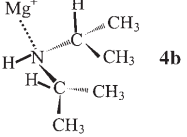
| Species | Energy ^[a] [hartree] | Bond length [Å] ^[b] | IE or BDE [kcal mol ⁻¹] ^[c] |
|--|------------------------------------|-----------------------------------|---|
| $(\text{CH}_3)_2\text{C}=\text{NH}_2^+$ (P-1a) | −173.55997 | 1.300 | 123.6 |
| $\text{CH}_3\text{CH}_2\text{CH}=\text{NH}_2^+$ (P-1b) | −173.54070 | 1.292 | – |
| $\text{CH}_3\text{CH}=\text{NH}_2^+$ (P-2) | −134.24882 | 1.291 | 133.1 |
| $\text{CH}_3\text{CH}_2\text{CH}_2\text{NH}=\text{CH}_2^+$ (P-3) | −212.81758 | 1.279 | 132.6 |
| $\text{CH}_3\text{CH}_2\text{CH}=\text{NH}(\text{n-C}_3\text{H}_7)^+$ (P-4) | −291.42175 | 1.288 | 119.5 |
| $\text{CH}_3\text{CH}=\text{NHCH}(\text{CH}_3)_2^+$ (P-5) | −252.13447 | 1.287 | 121.1 |
| $(\text{CH}_3)_2\text{CHNH}=\text{C}(\text{CH}_3)_2^+$ (P-6) | −291.43329 | 1.299 | – |
| Mg^+NHCH_3 (P-7) | −295.02214 | 1.931 | 46.6 |
| <i>cis</i> - $\text{Mg}^+\text{NHCH}_2\text{CH}_3$ (P-8a) | −334.32321 | 1.911 | 49.1 |
| <i>trans</i> - $\text{Mg}^+\text{NHCH}_2\text{CH}_3$ (P-8b) | −334.31700 | 1.933 | – |
| $\text{Mg}^+\text{NH}_2\text{CHCH}_3$ (P-8c) | −334.31719 | 2.090 | 38.3 |
| $\text{Mg}^+(\text{-NH}_2\text{CH}_2\text{CH}_2\text{-})$ (P-8d) | −334.35292 | 2.118 | 71.5 |
| <i>cis</i> - $\text{Mg}^+\text{NHCH}_2\text{CH}_2\text{CH}_3$ (P-9a) | −373.61737 | 1.903 | 52.3 |
| <i>trans</i> - $\text{Mg}^+\text{NH}(\text{n-C}_3\text{H}_7)$ (P-9b) | −373.60761 | 1.943 | – |
| <i>cis</i> - $\text{Mg}^+\text{NHCH}(\text{CH}_3)_2$ (P-10a) | −373.61914 | 1.916 | 51.9 |
| <i>trans</i> - $\text{Mg}^+\text{NHCH}(\text{CH}_3)_2$ (P-10b) | −373.61202 | 1.940 | – |

[a] ZPEs have been taken into account with a scaling factor of 0.989.

[b] C=N and Mg^+-N bond lengths for iminium cations and (Mg^+, N)-containing products, respectively. [c] The IEs are the ionization energies of imines for iminium species, BDEs are the Mg^+-N binding energies for the (Mg^+, N)-containing products.

$\text{CH}_2=\text{NH}_2^+$ (1.279 Å and 147.4 kcal mol⁻¹),^[7a,14] $\text{CH}_3\text{CH}=\text{NH}_2^+$ (**P-2**, 1.291 Å and 133.1 kcal mol⁻¹), and $(\text{CH}_3)_2\text{C}=\text{NH}_2^+$ (**P-1a**, 1.300 Å and 123.6 kcal mol⁻¹). However, *N*-alkyl substitution results in only a slight decrease in the IE, as seen in $\text{CH}_3\text{CH}_2\text{CH}_2\text{NH}=\text{CH}_2^+$ (**P-3**, 1.279 Å and 132.6 kcal mol⁻¹). In general, imines (see Table 2) have lower IEs than MgH and MgR (the calculated IEs are 143.0–163.7 kcal mol⁻¹, see Table S1) and this rationalizes the observation of iminium cations and $\text{MgR}(\text{H})$ rather than imines and $\text{MgR}(\text{H})$ cations.

Table 3. Calculated reaction energies for the photodissociation channels of $\text{Mg}^+-\text{NH}_2\text{CH}_2\text{CH}_2\text{CH}_3$ (**1a**), $\text{Mg}^+-\text{NH}_2\text{CH}(\text{CH}_3)_2$ (**2b**), $\text{Mg}^+-\text{NH}(\text{CH}_2\text{CH}_2\text{CH}_3)_2$ (**3**), and $\text{Mg}^+-\text{NH}[\text{CH}(\text{CH}_3)_2]_2$ (**4b**).

| Complexes | Photoproducts | Calculated reaction energies, ^[a] ΔE [kcal mol ⁻¹] |
|---|--|---|
|  1a | (1-1) $\text{Mg}^+ + \text{NH}_2\text{CH}_2\text{CH}_2\text{CH}_3$ | 44.5 |
| | (1-2) $\text{MgNH}_2^+ + \text{CH}_3\text{CH}_2\text{CH}_2\cdot$ | 70.4 |
| | (1-3) $\text{Mg}^+\text{NH}_3 + \text{CH}_3\text{CH}=\text{CH}_2$ | 23.0 |
| | (1-4) $\text{CH}_2\text{NH}_2^+ + \text{CH}_3\text{CH}_2\text{Mg}$ | 70.2 |
|  2b | (2-1) $\text{Mg}^+ + \text{NH}_2\text{CH}_2\text{CH}_2\text{CH}_3$ | 44.6 |
| | (2-2) $\text{MgNH}_2^+ + (\text{CH}_3)_2\text{CH}\cdot$ | 69.2 |
| | (2-3) $\text{Mg}^+\text{NH}_3 + \text{CH}_3\text{CH}=\text{CH}_2$ | 16.5 |
| | (2-4) $\text{CH}_3\text{CH}=\text{NH}_2^+ + \text{CH}_3\text{Mg}$ | 50.5 |
| | (2-5) $(\text{CH}_3)_2\text{C}=\text{NH}_2^+ + \text{MgH}$ | 44.4 |
|  3 | (3-1) $\text{Mg}^+ + \text{NH}(\text{CH}_2\text{CH}_2\text{CH}_3)_2$ | 47.2 |
| | (3-2) $\text{CH}_2\text{NH}_2^+ + \text{CH}_3\text{CH}_2\text{CH}_2\text{CH}_2\text{CH}_2\text{Mg}$ | 69.3 |
| | (3-2') $\text{CH}_2\text{NH}_2^+ + \text{MgCH}_2\text{CHCH}_3(\text{C}_2\text{H}_5)$ | 68.6 |
| | (3-3) $\text{Mg}^+\text{NH}_2\text{CH}_2 + \text{CH}_3\text{CH}_2\text{CH}_2\text{CH}_2\text{CH}_2\cdot$ | 78.0 |
| | (3-3') $\text{Mg}^+\text{NH}_2\text{CH}_2 + (\text{C}_2\text{H}_5)_3\text{CHCH}_2\cdot$ | 77.1 |
| | (3-4) $\text{Mg}^+\text{NH}_2\text{CH}_2\text{CH}_2 + \text{CH}_3\text{CH}_2\text{CH}_2\text{CH}_2\cdot$ | 50.1 |
| | (3-4') $\text{Mg}^+\text{NH}_2\text{CH}_2\text{CH}_2 + (\text{CH}_3)_2\text{CHCH}_2\cdot$ | 49.2 |
| | (3-5) $\text{Mg}^+\text{NHCH}_2\text{CH}_2\text{CH}_3 + \text{CH}_3\text{CH}_2\text{CH}_2\cdot$ | 72.1 |
|  4b | (3-6) $\text{CH}_3\text{CH}_2\text{CH}_2\text{NH}^+=\text{CH}_2 + \text{CH}_3\text{CH}_2\text{Mg}$ | 57.0 |
| | (3-7) $\text{CH}_3\text{CH}_2\text{CH}=\text{NHCH}_2\text{CH}_2\text{CH}_3^+ + \text{MgH}$ | 43.9 |
| | (4-1) $\text{Mg}^+ + \text{NH}[\text{CH}(\text{CH}_3)_2]_2$ | 47.2 |
| | (4-2) $\text{Mg}^+\text{CH}_3 + \text{CH}_3\text{CHNHCH}(\text{CH}_3)_2$ | 69.6 |
| | (4-3) $\text{CH}_3\text{CH}=\text{NH}_2^+ + \text{MgCHCH}_3(\text{C}_2\text{H}_5)$ | 48.8 |
| | (4-4) $(\text{CH}_3)_2\text{C}=\text{NH}_2^+ + (\text{CH}_3)_2\text{CHMg}$ | 34.4 |
| | (4-5) $\text{Mg}^+\text{NH}_2\text{CHCH}_3 + \text{C}_2\text{H}_5\text{CHCH}_3\cdot$ | 64.7 |
| | (4-6) $\text{Mg}^+\text{NHCH}(\text{CH}_3)_2 + (\text{CH}_3)_2\text{CH}\cdot$ | 55.6 |
| | (4-7) $\text{CH}_3\text{CH}=\text{NHCH}(\text{CH}_3)_2^+ + \text{MgCH}_3$ | 35.7 |
| | (4-8) $(\text{CH}_3)_2\text{C}=\text{NHCH}(\text{CH}_3)_2^+ + \text{MgH}$ | 32.3 |

[a] $\Delta E = E(\text{AB}) - E(\text{A}) - E(\text{B})$ was calculated at the B3LYP/6-31+G** level of theory at 0 K; the ZPE correction factor is 0.989.

The BDEs, bond lengths ($r_{\text{Mg-N}}$), and energies of the (Mg^+, N)-containing photoproducts, **P-7** to **P-10**, are listed in Table 2. Four isomeric structures for **P-8a-d** and two for **P-9a,b** and **P-10a,b** are considered. We find that for $\text{Mg}^+-\text{NHC}_n\text{H}_{2n+1}$ ($n \geq 2$), the alkyl-*cis*-to- Mg^+ structures (**P-8a** to **P-10a**) are always 4–6 kcal mol⁻¹ more stable than the *trans* forms (**P-8b** to **P-10b**), indicating a bonding interaction between Mg^+ and the alkyl group in the *cis* form. For **P-8**, **P-8d** is the most stable, being even more stable than the *cis* form (**P-8a**) by 18.6 kcal mol⁻¹. The Mg^+-N bond lengths of **P-8a** to **P-10a** were calculated to be about 1.90–1.93 Å, which are a little longer than that of Mg^+-NH_2 (1.901 Å).^[7a]

but much shorter than those of $\text{Mg}^+(\text{amines})$ (~2.16–2.19 Å).^[7] This shows that the Mg^+-N bond has a similarly strong covalent character to that of Mg^+-NH_2 . Correspondingly, the calculated BDEs of these photoproducts (Mg^+, N -containing) are as high as ~43.8–53.0 kcal mol⁻¹. Alkyl substitution at the α -carbon atom (**P-7**, **P-8a** to **P-10a**) also has an effect on the Mg^+-N bond lengths as well as the BDEs of Mg^+-NH_2 (54.2 kcal mol⁻¹).^[7] For example, the Mg^+-N bond length in $\text{Mg}^+-\text{NHCH}_3$ (**P-7**) is 1.931 Å (BDE = 46.6 kcal mol⁻¹)^[7] and decreases to 1.911 Å (BDE = 49.1 kcal mol⁻¹)^[7] in $\text{Mg}^+-\text{NHCH}_2\text{CH}_3$ (**P-8a**) and 1.903 Å (BDE = 52.3 kcal mol⁻¹)^[7] in $\text{Mg}^+-\text{NHCH}_2\text{CH}_2\text{CH}_3$ (**P-9a**). Exceptions include $\text{Mg}^+-\text{NHCH}(\text{CH}_3)_2$ (**P-10a**) ($r_{\text{Mg-N}} = 1.916$ Å) and $\text{Mg}^+-\text{NHCH}_3$ (**P-7**) in which the Mg^+-N bond is longer than that in **P-8a** and Mg^+-NH_2 even though they have one more CH_3 substitution at the α -carbon atom. This is apparently due to stronger inter-alkyl repulsion in **P-10a** than in **P-8a**.

C^α-H(C^β) activation: Note that MgH- and MgR- loss photoproducts (denoted by $[\text{L-H}]^+$ and $[\text{L-R}]^+$, respectively) are observed in all of the $\text{Mg}^+(\text{amine})$ systems except for $\text{Mg}^+-\text{NH}_2\text{CH}_2\text{CH}_2\text{CH}_3$ (Figure 3 and Figure 4, Table 1). In the $\text{Mg}^+(\text{amine})$ systems that have at least one β -carbon atom, the

photoreactions seem to proceed by $\text{C}^\alpha-\text{C}^\beta$ bond activation to yield MgR ($\text{R} = \text{CH}_3$ or CH_2CH_3) and the iminium cation (products **1-4**, **3-6**, **2-4**, and **4-7**, see Table 3). For example, in the first two reactions (**1-4** and **3-6**), MgCH_2CH_3 is eliminated following $\text{C}^\alpha-\text{C}^\beta$ bond activation, whereas in the last two (**2-4** and **4-7**), the eliminated neutral entity is MgCH_3 . Although a similar $\text{C}^\alpha-\text{C}$ bond activation reaction was previously observed in the photolysis of $\text{Mg}^+(\text{triethylamine})$,^[7b] the mechanism was not clear at the time owing to a dearth of data. This work has revealed more about the mechanism as we have now observed a richer variety of photoproducts that result from C-N , $\text{C}^\alpha-\text{C}$, and $\text{C}^\alpha-\text{H}$ bond activation. In

retrospect, the photoproduct $(\text{C}_2\text{H}_5)_2\text{N}=\text{CH}_2^+$ formed from the photolysis of Mg^+ (triethylamine) is actually a result of $\text{C}^\alpha\text{--C}$ bond activation rather than a further decomposition product of $[\text{N}(\text{C}_2\text{H}_5)_3]^+$ in the $\text{P}_{x,y}$ excitation region. The latter is now reassigned as a MgH elimination photoproduct, which is in accord with the photoreactions identified in the present work.

The products formed from loss of MgH are expected to be generated from $\text{C}^\alpha\text{--H}$ bond activation because the reaction is observed with Mg^+ (triethylamine), which has no amino hydrogen,^[7b] and with Mg^+ (methylamine, dimethylamine) complexes, which contain only $\text{C}^\alpha\text{--H}$ bonds.^[7a] Analogous hydride abstraction ($\text{C}^\alpha\text{--H}$ bond activation) from primary, secondary, and tertiary amines by various transition-metal ions such as Cu^+ , Ag^+ , Fe^+ , Co^+ , Ni^+ , Ru^+ , and Rh^+ has been established previously.^[15–24] In the work on the photolysis of $\text{Mg}^+\text{--NH}_2\text{CH}_3$ and $\text{Mg}^+\text{--NH}(\text{CH}_3)_2$, C--N insertion was observed only in the former, whereas $\text{C}^\alpha\text{--H}$ insertion was found in both cases. As there are no C--C bonds in these systems, one can conclude that $\text{C}^\alpha\text{--H}$ bond activation is favorable.^[7a] On the other hand, from our work on amine complexes with longer alkyl groups, $\text{C}^\alpha\text{--C}$ bond activation appears to compete strongly with $\text{C}^\alpha\text{--H}$ bond activation (see Figure 3, Figure 4, and Table 1).

To elucidate the $\text{C}^\alpha\text{--H}(\text{C}^\beta)$ bond activations, we traced the potential energy surface along selected reaction pathways of the Mg^+ (isopropylamine) (**2b**, see Figure 2) system, which has both H and CH_3 on the same side of the N--C bond as Mg^+ for metal-assisted activation of the $\text{C}^\alpha\text{--H}(\text{C}^\beta)$ bond. Figure 6 shows the calculated reaction pathways and potential energy profiles. From Figure 6 we find that the species generated from the $\text{C}^\alpha\text{--H}$ or $\text{C}^\alpha\text{--C}$ activation pathway are analogous to those generated from the C--H bond activation in Mg^+ (methylamine),^[7a14] which include the hydrogen-migrated species $\text{HMg}^+\text{--R1}$ from C--H bond activation (**a2**) or the analogous R-migrated species $\text{RMg}^+\text{--R2}$ (**a1**), charge-transfer species $[\text{MgH--R1}]^+$ (**b2**) or $[\text{MgR--R2}]^+$ (**b1**), and so on, suggesting that the two activations have a similar reaction mechanism.^[25]

In the abstraction of CH_3 or H from C^2 (i.e., C^α) of the amines, the $\text{C}^2\text{--N--Mg}^+\text{--C}^1(\text{H}^1)$ quadrangular transition states (**T2b-a1** and **T2b-a2**) are formed, which result from the migration of C^1H_3 and H^1 from C^2 in isopropylamine to Mg^+ , respectively (see Figure 6). In the transition-state structures, the $\text{Mg}^+\text{--C}^1(\text{H}^1)$ bond length (2.210(1.708) Å) is very close to that of free $\text{Mg}^+\text{--CH}_3(\text{H})$ and the $\text{C}^2\text{--C}^1(\text{H}^1)$ distance is 2.406–

(2.318) Å, indicating that the $\text{Mg}^+\text{--C}^1(\text{H}^1)$ bond is already formed and the $\text{C}^2\text{--C}^1(\text{H}^1)$ bond ruptured. Energetically, the two saddle points lie, respectively, about 50 and about 40 kcal mol^{-1} above the reactant complex **2b**, and are the highest energy barriers along the reaction channels. In the structures of the methyl- and hydrogen-migrated minima (**a1** and **a2**), the $\text{Mg}^+\text{--C}^1$ and $\text{Mg}^+\text{--H}^1$ distances are 2.070 and 1.667 Å, respectively, and the positive charge is on the MgCH_3 (MgH) entity in much the same way as it is in the photoinduced hydrogen migration in Mg^+ (methylamine).^[14] The $\text{N--Mg--C}^1(\text{H}^1)$ group is nearly linear, which results from sp hybridization centered on Mg^+ . This conformation favors the donation of the lone-pair electron on the nitrogen atom to $\text{MgCH}_3(\text{H})$ as well as reducing the repulsion between the two ligands which stabilizes the species. As a result, the minima are only about 25–30 kcal mol^{-1} above the reactant complex. Following the methyl or hydrogen migration, a charge-transfer minimum of $\text{MgCH}_3\text{--HN}^+\text{H}=\text{CHCH}_3$ (**b1**) or $\text{MgH--HN}^+\text{H}=\text{C}(\text{CH}_3)_2$ (**b2**) may be reached by the rotation of MgCH_3 or MgH (**Ta1-b1** and **Ta2-b2**). In the CT minima, the N--C^2 distances are 1.285–1.293 Å, consistent with the formation of iminium cations. Note that the CT minima share a common linear $\text{Mg--C}^1(\text{H}^1)\text{--H--N}$ structure, which is reminiscent of a hydrogen bond. In these species, the positive charge prefers to reside on the L--R (or L--H) group as found previously in a similar intermediate conformation (CT species) generated from the photodissociation of $\text{Mg}^+\text{--NH}_2\text{CH}_3$ in which the positive charge is located preferentially on the CH_2NH_2 entity.^[14] The CT between the iminium and MgH (or MgR) entities seems to be the key step in the reaction,^[14] which is driven by the peculiar stability of the iminium cation that results from its lower IE than those of MgH and MgR as mentioned above. Finally, homolysis of the bond results in the

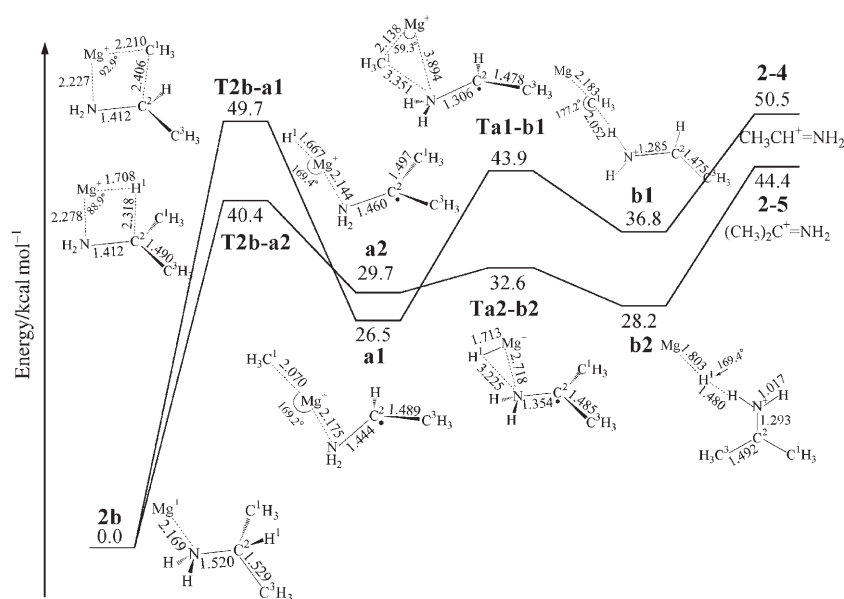


Figure 6. Schematic energy representation of $\text{C}^\alpha\text{--C}^\beta$ and $\text{C}^\alpha\text{--H}$ bond activations in trans-Mg^+ (isopropylamine) (**2b**). Bond lengths are in angstroms and bond angles are in degrees.

formation of MgCH_3 (or MgH) and the iminium cation, as observed. The appearance potentials (APs) of the $\text{C}^\alpha\text{--C}^\beta$ and $\text{C}^\alpha\text{--H}$ activation products (**2-4** and **2-5** in Table 3) formed from **2b** are calculated to be 50.5 and 44.4 kcal mol⁻¹, respectively, that is, less than the laser photon energy used in our experiments (~3.1 eV or 71.5 kcal mol⁻¹).

As shown in Table 3, although the APs of both products generated by the loss of MgCH_2CH_3 and MgCH_3 (**3-6** and **4-7**) from secondary amine complexes are clearly lower than those (**1-4** and **2-4**) derived from primary amine complexes, the MgR-loss products from the secondary amine complexes are not significantly enhanced (see Figure 3, Figure 4, and Table 1). This may be due to the strong competition of C–N activation in the secondary amine complexes as discussed below. For the $\text{C}^\alpha\text{--C}^\beta$ bond activation product Mg^+CH_3 formed from $\text{Mg}^+\text{--HN}[\text{CH}(\text{CH}_3)_2]_2$, the estimated formation energy of Mg^+CH_3 is 69.6 kcal mol⁻¹, which is less than the one-photon energy of the long wavelength range. The sum of the energies of routes **4-2** (Table 3) and the calculated BDE of $\text{Mg}^+\text{--CH}_3$ (44.3 kcal mol⁻¹) is 113.9 kcal mol⁻¹ (~251 nm) for the decomposition of Mg^+CH_3 , which is accessible in the short wavelength after taking account of thermal energies in the amine complexes. However, this ion is found to disappear in the short wavelength range perhaps as a result of state-specific effects resulting from a CT state.

C–N activation: To unveil the mechanistic details of C–N bond activation, we will first investigate the reaction paths that produce Mg^+NH_3 from Mg^+ (primary propylamine) and then move on to the intracomplex reactions that occur in secondary amine complexes.

To study the formation of Mg^+NH_2 and Mg^+NH_3 in Mg^+ (primary amine) complexes by C–N bond activation, **1a**, **1b**, and **2b** were used as model systems to survey the potential energy surfaces (PESs) along the reaction coordinates. The calculated reaction pathways and potential energy profiles are depicted in Figure 7. C–N insertion minima with a structure of $\text{R}^1\text{R}^2\text{HC--Mg}^+\text{--NH}_2$ (**c1** to **c3**) are formed by passing

through C–Mg–N triangular transition states (**T1a-c1**, **T1b-c2**, and **T2b-c3**). The stretched N–C¹ bonds (see Figure 7) may result from electron donation from the $3p_x$ orbital of Mg^{+*} to the σ_{CN}^* orbital as well as from σ_{CN} to $3s$ of Mg^{+*} , which is likely to induce internal conversion from the excited PES to the ground-state PES.^[26] These electron donations, although relatively weak for C–C or C–H bond activation for steric reasons, are expected to be strong for C–N activation because the interacting orbitals are approximately parallel to each other. In primary amine complexes, the $3p_z$ orbital of Mg^{+*} may also be involved in such an interaction with the help of the Mg–C–N scissor vibration, which is expected to be strongly excited owing to the unsymmetrical structures of the complexes. The relative energies of the saddle points are about 50–53 kcal mol⁻¹, which make them the highest crests along the reaction coordinates. With a de-

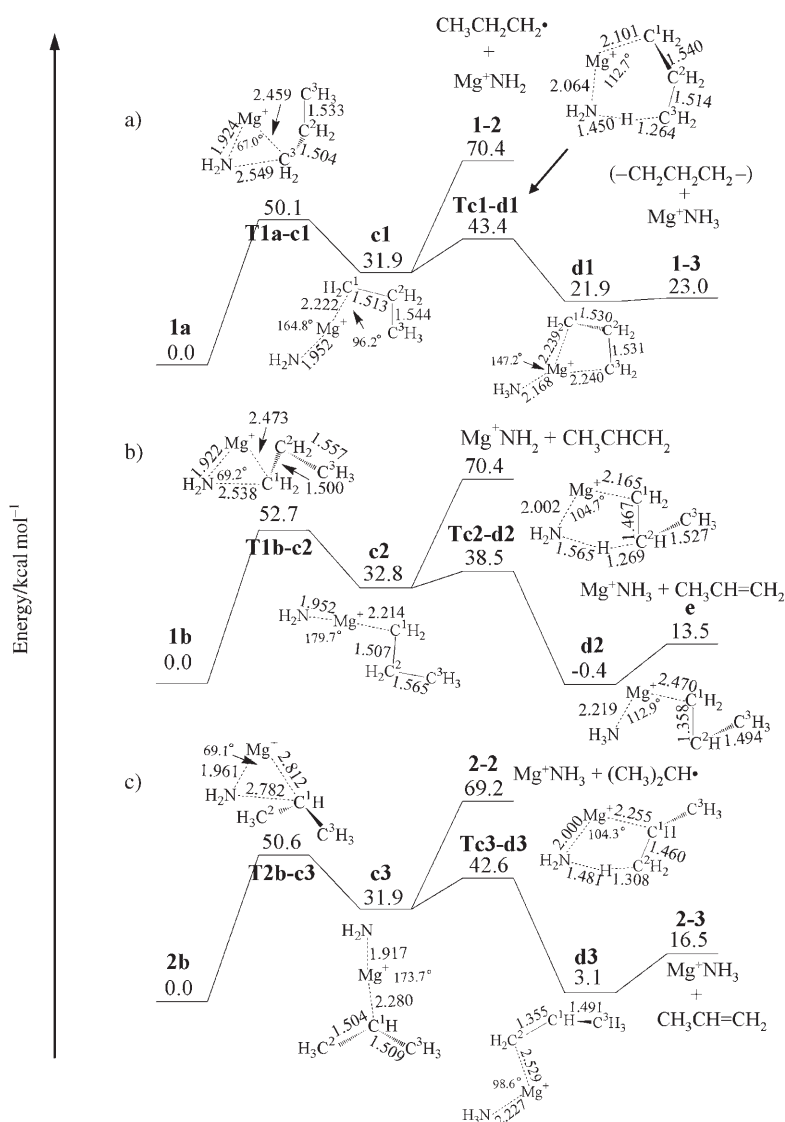


Figure 7. Schematic energy representation of C–N bond activation in a) *cis*- Mg^+ (propylamine) (**1a**), b) *trans*- Mg^+ (propylamine) (**1b**) and c) *trans*- Mg^+ (isopropylamine) (**2b**). Bond lengths are in angstroms and bond angles are in degrees.

crease in energy of about 20 kcal mol^{-1} , insertion minima **c1** to **c3** are produced. These minima have a linear $\text{N-Mg}^+-\text{C}^1$ structure, similar to the hydrogen-migrated species discussed above and is a common feature of two radicals connected through the sp-hybridized orbitals of Mg^+ .

The Mg^+ -insertion minima can take two possible routes along the reaction pathways. The first is the direct rupture of the Mg^+-C^1 bond to give $[\text{Mg}^+\text{NH}_2 + \text{R}^1\text{R}^2\text{HC}^1]$ (the Mg^+-N bond is too strong to be broken). The calculated APs for the formation of Mg^+NH_2 from the complexes are similar and are in the range of $69\text{--}71 \text{ kcal mol}^{-1}$, which is in effect less than the photon energy we used and thus explains their formation in the experiments. The other pathway involves a hydrogen shift to form Mg^+NH_3 , which has been identified in the photodissociation mass spectra of **1** and **2** (Figure 3 and Table 1). As Figure 7 shows, a hydrogen atom from both the γ - and β -carbon atoms can migrate to the nitrogen atom via five- ($\text{Mg}-\text{C}^\alpha-\text{C}^\beta-\text{H}-\text{N}$ as in **Tc2-d2** and **Tc3-d3**) and six-membered ($\text{Mg}-\text{C}^\alpha-\text{C}^\beta-\gamma\text{C}-\text{H}-\text{N}$ as in **Tc1-d1**) transition-state structures. Note that the $\text{C}^1-\text{Mg}-\text{N}$ bonds in the transition-state structures are significantly bent ($\sim 104\text{--}113^\circ$) from their linear precursors and this distortion can be accomplished with the help of the $\text{C}^\alpha-\text{Mg}-\text{N}$ scissor vibration, which is expected to be strongly excited after C–N insertion. Moreover, the energies of the transition states are relatively low ($38\text{--}44 \text{ kcal mol}^{-1}$ with respect to the corresponding reactants, see Figure 7). Passing through the transition states, the reaction systems find themselves in the deep valleys of $\text{H}_3\text{N}-\text{Mg}^+-\text{CH}_2=\text{CHCH}_3$ (**d2** and **d3**) and $\text{H}_3\text{N}-\text{Mg}^+(-\text{CH}_2\text{CH}_2\text{CH}_2-)$ (**d1**). In **d2** and **d3**, the $\text{N-Mg}-\text{C}^1$ unit has an angle of 112.9 and 98.6° , respectively. The angles are close to 90° , which is expected for complexes of Mg^+ with two closed-shell molecules,^[27–29] but are in contrast to those in **c1–c3**, **a1,a2**, and **b1,b2** with open-shell ligands. These precursors are analogous to the intermediate $(\text{C}_2\text{H}_4)\text{Co}^+(\text{NH}_3)$ detected in the reaction of Co^+CO with ethylamine, which may be formed by Co^+CO (Co^+ part) insertion into the C–N bond of ethylamine.^[15] Homolysis of the Mg^+-C bond yields Mg^+NH_3 and C_3H_6 (**1-3**, **e**, and **2-3**, see Figure 7), where C_3H_6 is cyclopropane for **1a** and $\text{CH}_3\text{CH}=\text{CH}_2$ for **1b** and **2b**. The formation energy of Mg^+NH_3 from **1a**, **1b**, and **2b** is calculated to be 23.0 , 13.5 , and $16.5 \text{ kcal mol}^{-1}$, respectively. These rather low formation energies of Mg^+NH_3 from Mg^+ (propylamine) suggest that after photoabsorption Mg^+NH_3 will have ample energy for further decomposition. Indeed, the formation energies of $\text{Mg}^+ + \text{NH}_3$ from **1a**, **1b**, and **2b** are merely ~ 61.6 , 52.1 , and $55.1 \text{ kcal mol}^{-1}$, respectively. Therefore it is not surprising to see that the yield of Mg^+NH_3 from the magnesium complexes (Figure 3 and Table 1) is very low at long wavelengths and even disappears at short wavelengths. In contrast, the formation energies of Mg^+NH_2 are much higher ($\sim 69.2 \text{ kcal mol}^{-1}$, see Table 3) and on top of this, the BDE of Mg^+-NH_2 ($51.0 \text{ kcal mol}^{-1}$) is also higher than that of Mg^+-NH_3 ($38.5 \text{ kcal mol}^{-1}$). This explains why the yield of the former is higher than that of the latter in the intracomplex photoreactions (see Figure 3 and Table 1).

The small iminium photoproducts formed from Mg^+ (di-propylamine) and Mg^+ (diisopropylamine) (e.g., $\text{Mg}^+(\text{NCH}_3)$, $\text{Mg}^+(\text{NC}_2\text{H}_5)$, CH_2NH_2^+ , and $\text{CH}_3\text{CHNH}_2^+$; Figure 4 and Table 1) cannot be formed simply by direct C–N or C–C bond activation without subsequent intracomplex bonding rearrangements. Clearly, the reactions leading to the formation of these products proceed in much the same way as the photoreactions leading to the loss of $\text{C}_3\text{H}_7^\cdot$ in Mg^+ (di-, triethylamine).^[7b] For illustration purposes, the $\text{C}_3\text{H}_7^\cdot$ -loss reaction in $\text{Mg}^+-\text{NH}(\text{C}_2\text{H}_5)_2$ is selected as a benchmark in our investigation. We surveyed reaction pathways starting with C–C and C–N bond activations. From the geometries of the species and the reaction energies given in the Supporting Information (Figures S3 and S4), we find that the pathway following the C–C bond activation and leading to $\text{C}_3\text{H}_7^\cdot$ loss is unreasonable both energetically and kinetically.^[30] Therefore, the C–C bond activation can be excluded as a tenable mechanism for $\text{C}_3\text{H}_7^\cdot$ loss from the photodissociation of $\text{Mg}^+-\text{NH}(\text{C}_2\text{H}_5)_2$. On the other hand, we found that C–N bond activation offers a reasonable path for this intriguing reaction. Through this reaction pathway, we obtain the reaction potential energy profile that is displayed in Figure 8. Although there are three isomers of Mg^+ (diethylamine) (**5** in Figure 8; **S-1** and **S-1a** in the Supporting Information, Figure S5), the staggered form was found to be the most stable structure at the B3LYP/6-31 + G** level of theory, lying 1.1 and $3.6 \text{ kcal mol}^{-1}$ below **S-1** (*trans*) and **S-1a** (*cis*), respectively. We therefore used the staggered form in our calculations.

As can be seen in Figure 8, the initial reactions for producing the $\text{CH}_2\text{CH}_2-\text{Mg}^+-\text{NH}_2(\text{CH}_2\text{CH}_3)$ minimum (**g**) from complex **5** are analogous to those shown in Figure 7 (from **1b** to **d2** and **2b** to **d3**). These include a low energy pathway of C–N bond activation via a triangular transition state (**T5-f**) followed by a β -hydrogen shift via a C^3 (or C^α)– $\text{Mg}-\text{N}-\text{H}^4-\text{C}^4$ (or C^β) five-membered-ring saddle point. The ethylene– Mg^+ –ethylamine minimum (**g**) is quite stable ($8.2 \text{ kcal mol}^{-1}$ above **5**) owing to strong $\text{Mg}^+-\text{C}_2\text{H}_4$ and $\text{Mg}^+-\text{NH}_2(\text{C}_2\text{H}_5)$ bonds. It is logical to reckon on a subsequent (β - or γ -)hydrogen shift following Mg^+ insertion into the C–N bond in amines, which induces the C–Mg–N scissor vibration. In primary amines, it is impossible to rearrange the hydrogen-shifted alkylene– Mg^+-NH_3 into a favorable cyclic intermediate except by breaking the C– Mg^+ bond, which leads to the formation of Mg^+NH_3 . For secondary or tertiary amines, however, the excited C–Mg–N scissor vibration in **g** will make C^4 in the ethylene moiety (activation position) abstract a methyl radical from the ethyl group in ethylamine via a six-membered-ring transition state (**Tg-h**). The transition state has the highest energy along the reaction pathway, and is located 82.8 and $6.7 \text{ kcal mol}^{-1}$, respectively, above the reactant and product. The energy is mostly less than the photon energy range we used except at the longest wavelength ($\sim 440 \text{ nm}$ or $65.0 \text{ kcal mol}^{-1}$). Even at the longest wavelength, the transition state may still be obtained as a result of the internal excitations of the $\text{Mg}^+-\text{NH}(\text{C}_2\text{H}_5)_2$ complex produced in our source. Following a de-

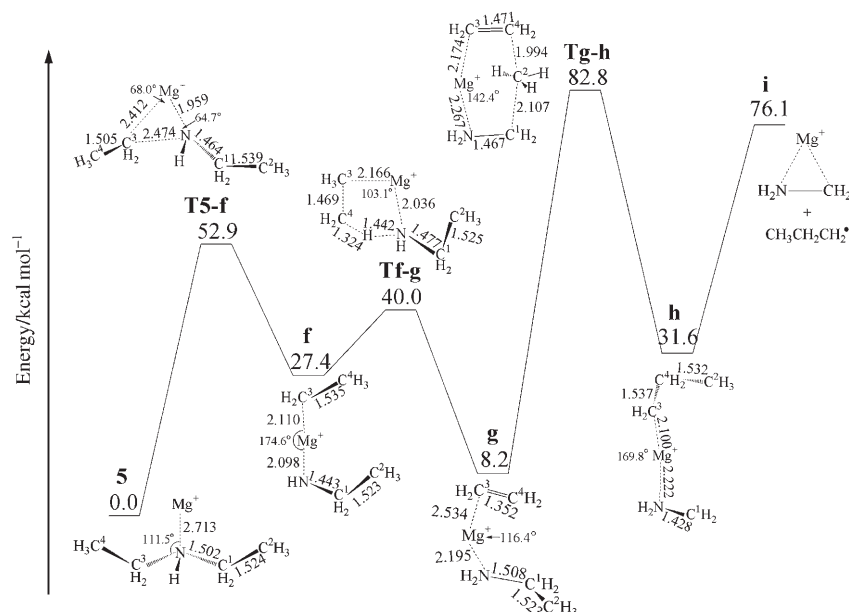


Figure 8. Schematic energy representation of C–N bond activation in $\text{Mg}^+(\text{diethylamine})$. Bond lengths are in angstroms and bond angles are in degrees.

crease in energy of $51.2 \text{ kcal mol}^{-1}$ a precursor minimum $\text{CH}_3\text{CH}_2\text{CH}_2\text{--Mg}^+\text{--NH}_2\text{CH}_2$ (**h**) is formed. Rupture of the $\text{Mg}^+\text{--C}^3$ bond ($\text{BDE} = 44.5 \text{ kcal mol}^{-1}$) yields the experimentally observed photoproducts $\text{CH}_3\text{CH}_2\text{CH}_2$ and $\text{Mg}^+\text{--NH}_2\text{CH}_2$. The appearance energy of the photoproduct is $76.1 \text{ kcal mol}^{-1}$.

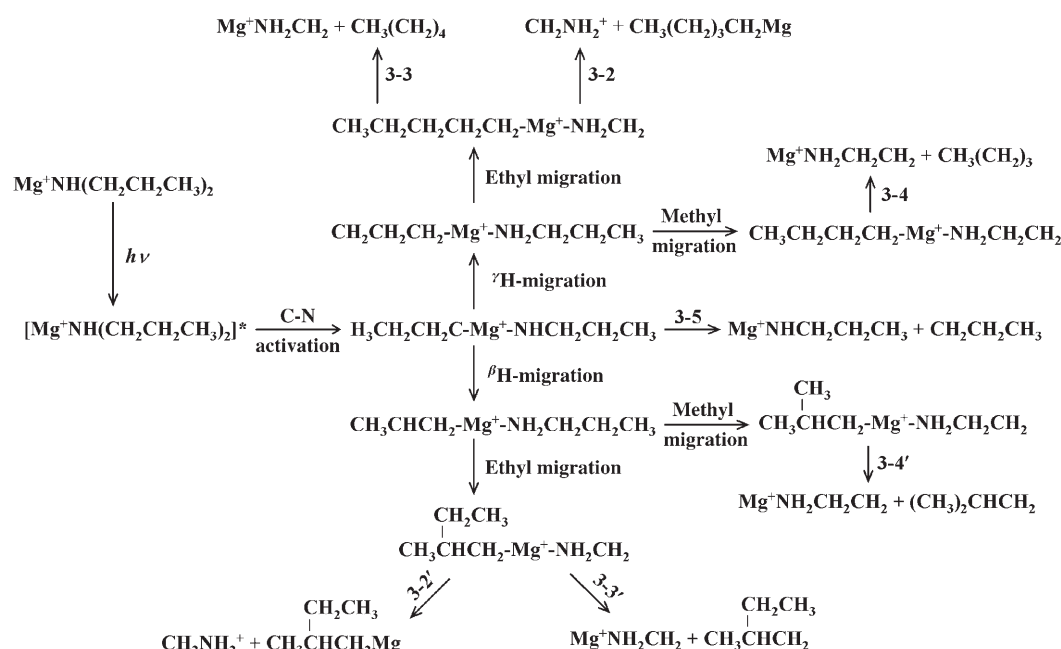
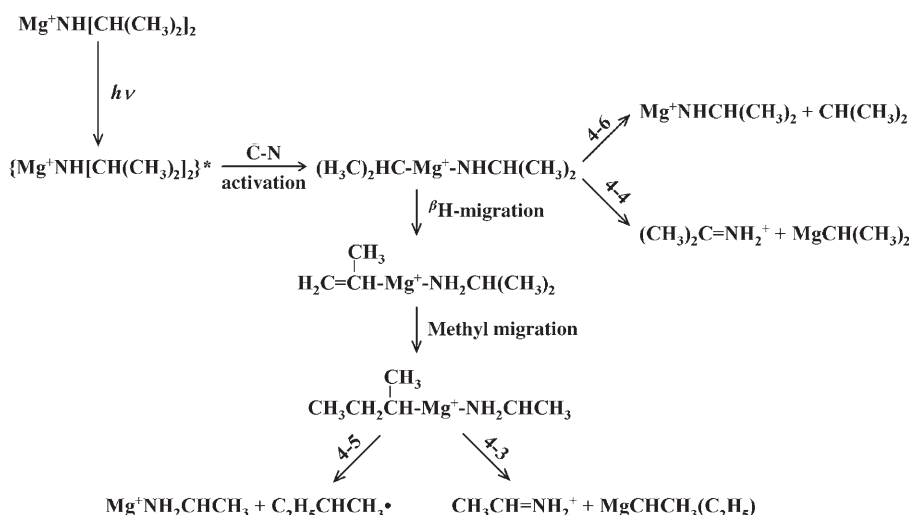
Although a full PES scan was not carried out for the Mg^+ (dipropylamine) complexes because of their relatively large size, C–N bond activation is expected to operate as well from an energy viewpoint. In view of the structural similarities of both the C–N insertion minima and the saddle points of the primary and secondary amine complexes, we expect that the energy differences between the saddle point and minima will be similar ($\sim 20 \text{ kcal mol}^{-1}$ in Figure 7). Thus in the following, we will only discuss the insertion minima. The likelihood of an insertion process $[\text{Mg}^+(\text{AB}) \rightarrow \text{A--Mg}^+\text{--B}]$ can be evaluated from the energy difference between the sum of the strengths of the two bonds formed, $\text{Mg}^+\text{--A}$ and $\text{Mg}^+\text{--B}$, and those of the two ruptured bonds, $\text{Mg}^+(\text{AB})$ and A--B . In going from the primary to secondary amine complexes, the BDEs of $\text{Mg}^+(\text{amine})$ increase by about 0.15 eV ($\sim 3.5 \text{ kcal mol}^{-1}$), while those of the C–N bonds decrease by about $5\text{--}15 \text{ kcal mol}^{-1}$ ($76.8/71.6$ and $75.5/60.3 \text{ kcal mol}^{-1}$ for **1a/3** and **2b/4b**, respectively). On the other hand, the $\text{Mg}^+\text{--NHCH}_2\text{CH}_2\text{CH}_3$ and $\text{Mg}^+\text{--NHCH}(\text{CH}_3)_2$ bonds (see Table 2) are about $2.3 \text{ kcal mol}^{-1}$ weaker than the $\text{Mg}^+\text{--NH}_2$ bond ($54.2 \text{ kcal mol}^{-1}$).^[7a] Moreover, the relevant C–N insertion minima have higher energies than the primary amine complexes by about 32 kcal mol^{-1} (Figure 7). Thus we can estimate that the analogous C–N insertion minima lie only about 28 and about 18 kcal mol^{-1} above the secondary amine complexes **3** and **4b**, respectively, meaning that C–N bond activation is more facile in the

secondary complexes. This might be another reason for the richer C–N activation photo-products produced from the secondary propylamine complexes. In the $\text{Mg}^+(\text{methylamine})$ complexes, however, C–N bond activation was observed in the photodissociation of $\text{Mg}^+\text{--NH}_2\text{CH}_3$ but not in the photodissociation of $\text{Mg}^+\text{--NH}(\text{CH}_3)_2$.^[7a] This may be explained by the fact that the $\text{Mg}^+\text{--NHCH}_3$ bond ($D_0 = 46.6 \text{ kcal mol}^{-1}$)^[7b] is weaker than that of $\text{Mg}^+\text{--NH}_2$ ($D_0 = 54.2 \text{ kcal mol}^{-1}$)^[7a] while the BDEs of the $\text{Mg}^+\text{--NH}_2\text{CH}_3$ and $\text{Mg}^+\text{--NH}(\text{CH}_3)_2$ bonds are similar.^[7a]

On the basis of the experimental and computational results presented above, we propose reaction branching path-

ways following C–N bond activation in $\text{Mg}^+(\text{dipropylamine})$ and $\text{Mg}^+(\text{diisopropylamine})$ (Scheme 1 and Scheme 2). For the C–N insertion minima $\text{XHN}\cdots\text{Mg}^+\cdots\text{X}$ ($\text{X} = \text{CH}_2\text{CH}_2\text{CH}_3$ or $\text{CH}(\text{CH}_3)_2$), as a result of the strong covalent character of the $\text{Mg}^+\text{--N}$ bond, the direct dissociation of these intermediates leads to the formation of Mg^+NHX . When $\text{X} = \text{CH}(\text{CH}_3)_2$, a hydrogen shift from the α -carbon to the nitrogen atom followed by CT with rotation of the $\text{MgCH}(\text{CH}_3)_2$ entity, as mentioned above, may be responsible for the observation of $(\text{CH}_3)_2\text{C}=\text{NH}_2^+$ in Figure 4a. A similar cation $\text{CH}_3\text{CH}_2\text{CH}=\text{NH}_2^+$ was not observed in $\text{Mg}^+\text{--HN}(\text{CH}_2\text{CH}_2\text{CH}_3)_2$. A plausible explanation for this is that $\text{CH}_3\text{CH}_2\text{CH}=\text{NH}_2^+$ (**P-1b**) is less stable than $(\text{CH}_3)_2\text{C}=\text{NH}_2^+$ (**P-1a**). The stable $(\text{CH}_3)_2\text{C}=\text{NH}_2^+$ (**P-1a**) drives the $\text{MgCH}(\text{CH}_3)_2$ entity in the insertion minimum to rotate following the hydrogen shift and to participate in the CT process as discussed above. The energies required for the formation of $\text{Mg}^+\text{--NHCH}_2\text{CH}_2\text{CH}_3$, $\text{Mg}^+\text{--NHCH}(\text{CH}_3)_2$, and $(\text{CH}_3)_2\text{C}=\text{NH}_2^+$ were computed to be 72.1 , 55.6 , and $34.4 \text{ kcal mol}^{-1}$, respectively (see products **3-5**, **4-6**, and **4-4** in Table 3), which are all accessible with one-photon excitation in the long-wavelength range ($\sim 440 \text{ nm}$, $\sim 65.0 \text{ kcal mol}^{-1}$). When possible internal excitations are considered,

Note that in the photodissociation of $\text{Mg}^+(\text{amine})$ complexes, only the bonds immediately connected to the α -carbon atoms, for example, $\text{C}^\alpha\text{--C}$, $\text{C}^\alpha\text{--H}$, and C--N , can be activated by $\text{Mg}^{+\ast}$. This is in contrast to the gas-phase reactions of transition-metal ions with amines, in which activations of $\text{C}^\beta\text{--C}^\gamma$, $\text{C}^\gamma\text{--C}^\delta$, etc., were also observed besides $\text{C}^\alpha\text{--C}^\beta$ bond activation.^[16] Clearly, the coordination of the nitrogen atom of the amine to Mg^+ plays a very important role here, which is manifested in terms of orbital-alignment and regiospecific effects.

Scheme 1. C-N activation branching pathways of Mg^+ (dipropylamine).Scheme 2. C-N activation branching pathways of Mg^+ (diisopropylamine).

State-specific effects: In the photodissociation of Mg^+ (secondary propylamine) complexes, small iminium cations (**3-2**, **3-2'**, **4-3** and **4-4**, see Table 3) and (Mg^+, N) -based fragments, including $\text{Mg}^+\text{NH}_2\text{C}_n\text{H}_{2n}$ ($n=1$ and 2) and $\text{Mg}^+\text{HNC}_n\text{H}_{2n+1}$ ($n=0$ and 3), are generated from C-N bond activation. From an energy point of view, the formation energy of $\text{Mg}^+ + \text{HNC}_n\text{H}_{2n+1}$ or $\text{Mg}^+ + \text{NH}_2\text{C}_n\text{H}_{2n}$ from the corresponding complex is the sum of the energies required for the generation of the (Mg^+, N) -based fragments and their subsequent dissociation. According to our calculations (Table 2 and Table 3), at least $\sim 114.1 \text{ kcal mol}^{-1}$ ($\sim 250 \text{ nm}$) is needed for

the formation of $\text{Mg}^+ + \text{NH}_2\text{CH}_2$,^[7b] $\text{Mg}^+ + \text{NH}_2\text{CH}_2\text{CH}_2$, and $\text{Mg}^+ + \text{NHCH}_2\text{CH}_2\text{CH}_3$ from **3**. This value ($114.1 \text{ kcal mol}^{-1}$) is near the wavelength limit (240 nm) used in our experiments. Moreover, the formation energies of $\text{Mg}^+ + \text{NH}_2\text{CHCH}_3$ and $\text{Mg}^+ + \text{NHCH}(\text{CH}_3)_2$ from the reactant complexes were evaluated to be 102.8 ($\sim 278 \text{ nm}$) and $107.5 \text{ kcal mol}^{-1}$ ($\sim 266 \text{ nm}$) from **4b**, respectively. It thus appears to us that the newly formed $\text{Mg}^+ + \text{NH}_2\text{C}_n\text{H}_{2n}$ ($n=1$ and 2) and $\text{Mg}^+\text{HNC}_3\text{H}_7$ might decompose at the short wavelength. However, this is not supported by the following observations. First, Mg^+NH_2 is clearly observed in the short-wavelength range for

$\text{Mg}^+(\text{H}_2\text{NCH}_2\text{CH}_2\text{CH}_3)$ and $\text{Mg}^+[\text{H}_2\text{NCH}(\text{CH}_3)_2]$ (see Figure 3 and Table 1) although a similar amount of energy ($\sim 119.9 \text{ kcal mol}^{-1}$) is needed for the formation of $\cdot\text{NH}_2$ from the two complexes. Second, no (Mg^+, N) -based fragments were observed at an energy lower than the P_z excitation of $\text{Mg}^+-\text{HN}(\text{CH}_2\text{CH}_2\text{CH}_3)_2$ and $\text{Mg}^+[\text{H}_2\text{NCH}(\text{CH}_3)_2]$ (e.g., 280 nm , $\approx 101.9 \text{ kcal mol}^{-1}$). Third, the C-N bond activation products like $\text{CH}_2=\text{NH}_2^+$ and $\text{CH}_3\text{CH}=\text{NH}_2^+$ from $\text{Mg}^+-\text{HN}(\text{CH}_2\text{CH}_2\text{CH}_3)_2$ and $\text{Mg}^+-\text{HN}[\text{CH}(\text{CH}_3)_2]_2$ also disappear in the short-wavelength range though they are unlikely to dissociate. As a result, the sudden disappearance of

$\text{Mg}^+-\text{NH}_2\text{C}_n\text{H}_{2n}$ ($n=1$ and 2) and $\text{Mg}^+-\text{HNC}_3\text{H}_7$ in the short-wavelength range is not due to their consecutive decomposition but more probably as a result of state-specific effects.

These state-specific effects can be understood in terms of the orbital alignments in the secondary amine complexes. As Figure 2 shows, the p_z orbital of Mg^+ in complexes **3** and **4** is roughly perpendicular to those of the C–N bonds. Therefore, no C–N bond activation photoproducts are likely to be formed from the P_z excitation because Mg^+ simply cannot insert into the C–N bond, whereas the $p_{x,y}$ orbitals of Mg^+ can interact with the σ^* orbital of the C–N bond and the $3s$ orbital with the σ orbital because they are roughly parallel to each other. This is in marked contrast to the case of the Mg^+ (primary amine) complexes, in which the unsymmetrical structures of the parent complexes (Figure 2) lead to the state nonspecificity of the C–N bond activation as discussed above.

Note that the (Mg^+, N) -based fragments derived from secondary amine complexes cannot decompose further to Mg^+ in the $3^2P_{x,y}$ excitation region owing to a lack of energy, whereas for the primary amine complexes, the photoproduct Mg^+NH_3 has ample energy to dissociate, as mentioned above. This may be the reason why relatively rich and abundant C–N activation products are formed from the secondary amine complexes in the $3^2P_{x,y}$ excitation region (see Figure 4a and Table 1), whereas Mg^+ is predominant over the C–N activation products for the primary amine complexes (see Figure 3a and Table 1).

Inter-alkyl C–C coupling reactions: The intracomplex C–C coupling reactions in the secondary amine complexes are rather intriguing and merit special discussion. In general, C–C coupling reactions assisted by catalysts have a special position in organic chemistry. A classic example is the well-known Ziegler–Natta type C–C bond formation involving C=C insertion into metal–ligand bonds, which is directly relevant to the catalysis of alkene polymerization.^[31–35] On the surface, the C–C coupling reactions we observed can originate from both C–N and C–C bond activation because both these bonds are cleaved anyway during the reactions. It turns out that Mg^+ insertion into the C–N bond is the key step, as discussed above, based on the calculation of the C_3H_7 -loss channel in the photodissociation of Mg^+ (diethylamine).

We identified a hydrogen-shift process following Mg^+ insertion into the C–N bond of amines with long N -alkyl group(s) (two carbon atoms or above owing to the need to form a ring transition state with at least five members). For primary amine complexes, the hydrogen shift leads to the generation of Mg^+NH_3 , as observed in the photodissociation mass spectra of Mg^+ (propylamine) and Mg^+ (isopropylamine) (Figure 3 and Table 1). It is shown in Figure 7 that this reaction path is both energetically and kinetically favorable following Mg^+ insertion into the C–N bond. The insertion minima (relative to the parent complexes) derived from secondary amine complexes are about 4–14 kcal mol^{−1} lower

in energy than those derived from primary amine complexes, and both $\text{Mg}^+-\text{NH}_2\text{CH}_2\text{CH}_2\text{CH}_3$ (**1a**) and $\text{Mg}^+-\text{NH}_2\text{CH}(\text{CH}_3)_2$ (**2b**) bonds are about 6 kcal mol^{−1} stronger than the Mg^+-NH_3 bond. Thus the hydrogen-shift minima from Mg^+ (dipropylamine) complexes are estimated to lie 20 and 11 kcal mol^{−1} above the parent complexes **3** and **4b**, respectively, considering that the hydrogen-shifted minima (**d1** and **d3**) lie about 22 and 3 kcal mol^{−1} above the Mg^+ (primary propylamine) complexes **1a** and **2b** (see Figure 7). Therefore, hydrogen shifts are also energetically possible in the secondary amine complexes following Mg^+ insertion into the C–N bond.

For secondary (or tertiary) amine complexes, however, there is a possibility that C–C coupling will occur following the hydrogen-shift process leading to the formation of three photoproducts from Mg^+ (dipropylamine) ($\text{CH}_2=\text{NH}_2^+$, $\text{Mg}^+-\text{NH}_2\text{CH}_2$, and $\text{Mg}^+-\text{NH}_2\text{CH}_2\text{CH}_2$) and two from Mg^+ (diisopropylamine) ($\text{CH}_3\text{CH}=\text{NH}_2^+$ and $\text{Mg}^+-\text{NH}_2\text{CHCH}_3$) (Figure 4a and Table 1). Note that these photoproducts cannot be formed simply by direct C–N or C–C bond activation without subsequent rearrangements. It is gratifying to find that these reactions share the same mechanism as the C_3H_7 -loss reactions in Mg^+ (di-, triethylamine) (Figure 8). As Scheme 1 shows, analogous to the case of Mg^+ (propylamine), both β - and γ -hydrogen shifts are possible following C–N bond activation in Mg^+ (dipropylamine). $\text{Mg}^+-\text{NH}_2\text{CH}_2$ (loss of $\text{C}_5\text{H}_{11}^+$), $\text{CH}_2=\text{NH}_2^+$ (loss of $\text{MgC}_5\text{H}_{11}$), and $\text{Mg}^+-\text{NH}_2\text{CH}_2\text{CH}_2$ (loss of C_4H_9^+) are expected to form after the subsequent ethyl and methyl migrations, respectively. For Mg^+ (diisopropylamine), as shown in Scheme 2, C–N activation is followed by a β -hydrogen shift and methyl migration, which are responsible for the production of $\text{Mg}^+-\text{NH}_2\text{CHCH}_3$ (loss of C_4H_9^+) and $\text{CH}_3\text{CH}=\text{NH}_2^+$ (loss of MgC_4H_9). The APs for these intracomplex C–C coupling photoproducts are all less than the laser photon energy used in our experiments (see Table 3).

A legitimate question is whether C_4H_9^+ and $\text{C}_5\text{H}_{11}^+$ are really the ultimate products formed in the process illustrated in Scheme 1. The answer is a positive one. In fact, according to the calculations, all of the products except $\text{Mg}^+-\text{NH}_2\text{CH}_2\text{CH}_2$ from Mg^+ (dipropylamine) are energetically inaccessible by one-photon excitation according to the APs of **3-3**, **3-3'**, and **4-5** (see Table 3) and the dissociation energy of the C–C bond in the alkyl radical (~ 25 kcal mol^{−1}).^[7b] For $\text{Mg}^+-\text{NH}_2\text{CH}_2\text{CH}_2$, a sequential loss mechanism is also possible because the energy threshold for sequential alkyl+alkene loss is estimated to be 75 kcal mol^{−1} on the basis of the APs of **3-4** and **3-4'** (50.0 and 49.1 kcal mol^{−1}) and the dissociation energy of C_4H_9^+ to C_3H_6 and CH_3^+ (~ 25 kcal mol^{−1}), which is accessible by one-photon excitation. However, we believe that the C–C coupling reaction is the most likely process for the following reasons. First, all of the analogous reactions have been shown to occur by C–C coupling, as discussed above. Secondly, the sequential loss process instead of the C–C coupling reaction seems to be inexplicable. For example, although the rupture of the propylene-(or -cyclopropane-) $\text{Mg}^+(n\text{-propylamine})$ bond (minima

similar to **g** in Figure 8, or **d1** and **d2** in Figure 7) to lose C_3H_6 as a result of C–N bond activation is reasonable, subsequent $\text{Mg}^+\text{--NH}_2\text{CH}_2\text{CH}_2\text{--CH}_3$ bond cleavage for the second step is more difficult to understand because the ruptured bond is far away from the bond activation center.

Conclusions

This work on $\text{Mg}^+(n\text{-propyl, isopropylamines})$ has advanced our studies on photoinduced reactions in $\text{Mg}^+(\text{alkylamines})$. By combining the extensive experimental and computational efforts, the mechanisms of the photoreactions of these complexes have started to unfold. The photoreactions appear to start with the activation of mainly the $\text{C}^\alpha\text{--C}$ and C–N bonds by Mg^+ , and less so, the $\text{C}^\alpha\text{--H}$ bond, following the electronic excitation of Mg^+ ($3^2\text{P} \leftarrow 3^2\text{S}$) through photoabsorption. We can now conclude by summarizing a number of the main points below.

- 1) In the long-wavelength range, only the bonds immediately connected to the α -carbon atoms in $\text{Mg}^+(\text{amine})$ complexes, for example, $\text{C}^\alpha\text{--C}$, $\text{C}^\alpha\text{--H}$, and C–N, can be activated by Mg^{+*} . C–N bond activation is more facile than $\text{C}^\alpha\text{--C}$ bond activation in the photodissociation of secondary propylamine complexes and the evaporative formation of Mg^+ is a comparable reaction channel. For the primary amine complexes, however, the $\text{C}^\alpha\text{--C}$ bond-cleavage photoproducts are similar to those formed by C–N bond cleavage, and both are overwhelmed by the photofragment Mg^+ . $\text{C}^\alpha\text{--H}$ bond-activation photoproducts are observed in all of the amine complexes we have studied except in $\text{Mg}^+(\text{propylamine})$ but in general they are considered as minor products.
- 2) In the short-wavelength range, products generated from $\text{C}^\alpha\text{--C}$ rupture are always observed in the photodissociation of the $\text{Mg}^+(\text{propylamine})$ complexes. For $\text{Mg}^+(\text{primary amines})$, the iminium photoproducts resulting from $\text{C}^\alpha\text{--C}$ cleavage prevail upon excitation of the P_z and CT states of Mg^+ , whereas in $\text{Mg}^+(\text{secondary amines})$, $\text{C}^\alpha\text{--C}$ cleavage is a minor process compared with the evaporation channel. C–N activation products, although much less abundant, are also observed in primary amine complexes in this spectral region.
- 3) The photodissociation of $\text{Mg}^+(\text{primary amine})$ complexes with long N -alkyl chains has revealed a subsequent step following the insertion of Mg^+ into the C–N bond in amines, that is, a (β - or γ -)hydrogen shift leading to the formation of a quite stable $\text{NH}_3\text{--Mg}^+\text{--alkene}$ intermediate. $\text{Mg}^+\text{--NH}_3$ is produced by homolysis of the $\text{Mg}^+\text{--alkene}$ bond. This is a reaction channel with very low reaction energies.
- 4) Further N -alkyl substitution in alkylamines gives rise to a novel intracomplex C–C coupling photoreaction. For example, photodissociation of $\text{Mg}^+(\text{secondary amines})$ follows an intracomplex C–C coupling photoreaction pathway after C–N bond activation and the subsequent (β -, or γ -)hydrogen shift. This reaction pathway domi-

nates the $\text{C}^\alpha\text{--C}$ and $\text{C}^\alpha\text{--H}$ activation channels upon $\text{P}_{x,y}$ excitation of Mg^+ .

- 5) Both $\text{C}^\alpha\text{--C}$ and $\text{C}^\alpha\text{--H}$ bond activations share a common reaction mechanism—a three-step process involving H(R) migration, CT, and decomposition. The driving force for this process is dictated by the special stability of the iminium cations, which arise from the low IEs of their precursors relative to those of their partners, metal hydrides (MgH) and metal-alkyls (MgR).

Acknowledgements

This work was supported by an RGC grant administered by the UGC of Hong Kong and the Key Project of the Chinese Ministry of Education (NO. 104119). W.Y.G. is grateful to the National Natural Science Foundation of China (Grant No. 20476061) for financial support. Support from HKUST and CUP is also gratefully acknowledged.

- [1] M. A. Duncan, *Ann. Rev. Phys. Chem.* **1997**, *48*, 69.
- [2] P. D. Kleiber, J. Chen, *Int. Rev. Phys. Chem.* **1998**, *17*, 1.
- [3] K. Fuke, K. Hashimoto, S. Iwata, *Adv. Chem. Phys.* **1999**, *110*, 431.
- [4] M. T. Rodgers, P. B. Armentrout, *Mass Spectrom. Rev.* **2000**, *19*, 215.
- [5] J. M. Farrar, *Int. Rev. Phys. Chem.* **2003**, *22*, 593.
- [6] a) H. C. Liu, X. H. Zhang, C. S. Wang, W. Y. Guo, Y. D. Wu, S. H. Yang, *J. Phys. Chem. A* **2004**, *108*, 3356; b) H. C. Liu, J. L. Sun, Y. H. Hu, K. L. Han, S. H. Yang, *Chem. Phys. Lett.* **2004**, *389*, 342; c) H. C. Liu, S. H. Yang, X. H. Zhang, Y. D. Wu, *J. Am. Chem. Soc.* **2003**, *125*, 12351; d) H. C. Liu, C. S. Wang, W. Y. Guo, Y. D. Wu, S. H. Yang, *J. Am. Chem. Soc.* **2002**, *124*, 3794.
- [7] a) W. Y. Guo, H. C. Liu, S. H. Yang, *J. Chem. Phys.* **2002**, *117*, 6061; b) W. Y. Guo, H. C. Liu, S. H. Yang, *J. Chem. Phys.* **2002**, *116*, 2896.
- [8] X. Yang, K. L. Gao, H. C. Liu, S. H. Yang, *J. Chem. Phys.* **2000**, *112*, 10236.
- [9] Gaussian 03 (Revision B.05), M. J. Frisch, G. W. Trucks, H. B. Schlegel, G. E. Scuseria, M. A. Robb, J. R. Cheeseman, J. A. Montgomery, Jr., T. Vreven, K. N. Kudin, J. C. Burant, J. M. Millam, S. S. Iyengar, J. Tomasi, V. Barone, B. Mennucci, M. Cossi, G. Scalmani, N. Rega, G. A. Petersson, H. Nakatsuji, M. Hada, M. Ehara, K. Toyota, R. Fukuda, J. Hasegawa, M. Ishida, T. Nakajima, Y. Honda, O. Kitao, H. Nakai, M. Klene, X. Li, J. E. Knox, H. P. Hratchian, J. B. Cross, C. Adamo, J. Jaramillo, R. Gomperts, R. E. Stratmann, O. Yazyev, A. J. Austin, R. Cammi, C. Pomelli, J. W. Ochterski, P. Y. Ayala, K. Morokuma, G. A. Voth, P. Salvador, J. J. Dannenberg, V. G. Zakrzewski, S. Dapprich, A. D. Daniels, M. C. Strain, O. Farkas, D. K. Malick, A. D. Rabuck, K. Raghavachari, J. B. Foresman, J. V. Ortiz, Q. Cui, A. G. Baboul, S. Clifford, J. Cioslowski, B. B. Stefanov, G. Liu, A. Liashenko, P. Piskorz, I. Komaromi, R. L. Martin, D. J. Fox, T. Keith, M. A. Al-Laham, C. Y. Peng, A. Nanayakkara, M. Challacombe, P. M. W. Gill, B. Johnson, W. Chen, M. W. Wong, C. Gonzalez, J. A. Pople, Gaussian, Inc., Pittsburgh, PA, **2003**.
- [10] a) A. D. Becke, *J. Chem. Phys.* **1993**, *98*, 5648; b) C. Lee, W. Yang, R. G. Parr, *Phys. Rev. B* **1988**, *37*, 785.
- [11] J. B. Foresman, Æ. Frisch, *Exploring Chemistry with Electronic Structure Methods*, 2nd ed., Gaussian, Pittsburgh, **1996**, p. 64.
- [12] a) T. Bally, G. N. Sastry, *J. Phys. Chem. A* **1997**, *101*, 7923; b) T. D. Crawford, E. Kraka, J. F. Stanton, D. Cremer, *J. Chem. Phys.* **2001**, *114*, 10638; c) N. Koga, K. Morokuma, *J. Am. Chem. Soc.* **1991**, *113*, 1907; d) J. M. Galbraith, P. R. Schreiner, N. Harris, W. Wei, A. Wittkopp, S. Shaik, *Chem. Eur. J.* **2000**, *6*, 1446; e) J. Grafenstein, A. M. Hjerpe, E. Kraka, D. Cremer, *J. Phys. Chem. A* **2000**, *104*, 1748; f) E. Kraka, J. Anglada, A. Hjerpe, M. Filatov, D. Cremer, *Chem. Phys. Lett.* **2001**, *348*, 115.

- [13] a) B. Braïda, S. Hazebrucq, P. C. Hiberty, *J. Am. Chem. Soc.* **2002**, *124*, 2371; b) P. C. Hiberty, S. Humbel, P. Archirel, *J. Phys. Chem.* **1994**, *98*, 11 697; c) B. Braïda, P. C. Hiberty, A. Savin, *J. Phys. Chem. A* **1998**, *102*, 7872; d) B. Braïda, D. Lauvergnat, P. C. Hiberty, *J. Chem. Phys.* **2001**, *115*, 90.
- [14] W. Y. Guo, X. Q. Lu, S. Q. Hu, S. H. Yang, *Chem. Phys. Lett.* **2003**, *381*, 109.
- [15] B. D. Radecki, J. Allison, *J. Am. Chem. Soc.* **1984**, *106*, 946.
- [16] S. W. Buckner, B. S. Freiser, *J. Am. Chem. Soc.* **1987**, *109*, 4175.
- [17] S. J. Babinec, J. Allison, *J. Am. Chem. Soc.* **1984**, *106*, 7718.
- [18] S. W. Sigsworth, A. W. Castleman, Jr., *J. Am. Chem. Soc.* **1989**, *111*, 3566.
- [19] M. A. Tolbert, J. L. Beauchamp, *J. Phys. Chem.* **1986**, *90*, 5015.
- [20] S. W. Buckner, J. R. Gord, B. S. Freiser, *J. Chem. Phys.* **1988**, *88*, 3678.
- [21] S. Karrass, T. Prüsse, K. Eller, H. Schwarz, *J. Am. Chem. Soc.* **1989**, *111*, 9018.
- [22] a) S. Karrass, K. Eller, C. Schulze, H. Schwarz, *Angew. Chem.* **1989**, *101*, 634; *Angew. Chem. Int. Ed. Engl.* **1989**, *28*, 607.
- [23] S. Karrass, K. Eller, H. Schwarz, *Chem. Ber.* **1990**, *123*, 939.
- [24] K. Eller, H. Schwarz, *Chem. Rev.* **1991**, *91*, 1121.
- [25] The geometries and energies for C⁺–C activation leading to MgCH₂CH₃ loss from Mg⁺–NH(CH₂CH₂CH₃) are shown in Figures S1 and S2 (Supporting Information), respectively. A three-step process is thought to occur, which includes H(R) migration, charge transfer, and decomposition (see Figure 6). Here it is shown that MgCH₂CH₃ loss exhibits the reaction mechanism involved in the loss of MgCH₃ or MgH.
- [26] a) L. N. Ding, M. Young, P. D. Kleiber, W. C. Stwalley, A. M. Lyyra, *J. Phys. Chem.* **1993**, *97*, 2181; b) L. N. Ding, P. D. Kleiber, M. A. Young, W. C. Stwalley, A. M. Lyyra, *Phys. Rev. A* **1993**, *48*, 2024.
- [27] a) J. E. Reddic, M. A. Duncan, *J. Chem. Phys.* **1999**, *110*, 9948; b) J. E. Reddic, S. H. Pullins, M. A. Duncan, *J. Chem. Phys.* **2000**, *112*, 4974; c) C. S. Yeh, K. F. Willey, D. L. Robbins, M. A. Duncan, *Int. J. Mass Spectrom. Ion Processes* **1994**, *131*, 307; d) C. T. Scurlock, S. H. Pullins, M. A. Duncan, *J. Chem. Phys.* **1996**, *105*, 3579; e) D. L. Robbins, L. R. Brock, L. S. Pilgrim, M. A. Duncan, *J. Chem. Phys.* **1995**, *102*, 1481; f) K. N. Kirschner, B. Ma, J. P. Bowen, M. A. Duncan, *Chem. Phys. Lett.* **1998**, *295*, 204; g) C. S. Yeh, K. F. Willey, D. L. Robbins, M. A. Duncan, *Chem. Phys. Lett.* **1992**, *196*, 233; h) K. F. Willey, C. S. Yeh, D. L. Robbins, J. S. Pilgrim, M. A. Duncan, *J. Chem. Phys.* **1992**, *97*, 8886; i) C. T. Scurlock, S. H. Pullins, M. A. Duncan, *J. Chem. Phys.* **1996**, *104*, 4591; j) M. R. France, S. H. Pullins, M. A. Duncan, *Chem. Phys.* **1998**, *239*, 447; k) J. E. Reddic, M. A. Duncan, *Chem. Phys. Lett.* **1999**, *312*, 96; l) M. R. France, S. H. Pullins, M. A. Duncan, *J. Chem. Phys.* **1998**, *109*, 8842; m) S. S. Wesolowski, A. K. Rollin, H. F. Schaefer III, M. A. Duncan, *J. Chem. Phys.* **2000**, *113*, 701.
- [28] a) F. Misaizu, M. Sanekata, K. Tsukamoto, K. Fuke, S. Iwata, *J. Phys. Chem.* **1992**, *96*, 8259; b) F. Misaizu, M. Sanekata, K. Tsukamoto, K. Fuke, S. Iwata, *J. Chem. Phys.* **1994**, *100*, 1161; c) H. Watanabe, S. Iwata, K. Hashimoto, F. Misaizu, K. Fuke, *J. Am. Chem. Soc.* **1995**, *117*, 755; d) M. Sanekata, F. Misaizu, F. Fuke, S. Iwata, K. Hashimoto, *J. Am. Chem. Soc.* **1995**, *117*, 747; e) M. Sanekata, F. Misaizu, K. Fuke, *J. Chem. Phys.* **1996**, *104*, 9768.
- [29] a) X. Yang, Y. H. Hu, S. H. Yang, *Chem. Phys. Lett.* **2000**, *322*, 491; b) X. Yang, Y. H. Hu, S. H. Yang, *J. Phys. Chem. A* **2000**, *104*, 8496; c) X. Yang, H. C. Liu, S. H. Yang, *J. Chem. Phys.* **2000**, *113*, 3111; d) X. Yang, K. L. Gao, H. C. Liu, S. H. Yang, *J. Chem. Phys.* **2000**, *112*, 10236; e) W. Y. Lu, S. H. Yang, *J. Phys. Chem. A* **1998**, *102*, 825; f) H. C. Liu, W. Y. Guo, S. H. Yang, *J. Chem. Phys.* **2001**, *115*, 4612.
- [30] The geometries and energies involved in the C–C coupling reactions following the C–C activation in Mg⁺–NH(C₂H₅)₂ are shown in Figures S3 and S4 (Supporting Information), respectively. It can be seen that this channel is unreasonable both energetically and kinetically. For example, the route is expected to involve a hydrogen migration (**S-a**→**S-b**) with a barrier of 101.3 kcal mol^{−1} (Figure S4), which is much higher than the experimental photon energy (~440 nm or 65.0 kcal mol^{−1}). For the subsequent C₂H₅ migration (**S-b**→**S-d**), no transition states bridging the minima **S-b** and **S-c** as well as **S-c** and **S-d** could be located. Moreover, the hydrogen migration (**S-Ta-b**) does not seem to be kinetically reasonable (Figure S3) because there is no driving force for rupture of the C⁺–H bond to form **S-Ta-b** from **S-a**.
- [31] a) Y. Huang, Y. D. Hill, B. S. Freiser, *J. Am. Chem. Soc.* **1991**, *113*, 840; b) Y. Huang, Y. D. Hill, M. Sodupe, C. W. Bauschlier, Jr., B. S. Freiser, *J. Am. Chem. Soc.* **1992**, *114*, 9106.
- [32] B. C. Guo, A. W. Castleman, Jr., *J. Am. Chem. Soc.* **1992**, *114*, 6152.
- [33] P. Corradini, G. Guerra, L. Cavallo, *Acc. Chem. Res.* **2004**, *37*, 231.
- [34] M. C. Baird, *Chem. Rev.* **2000**, *100*, 1471.
- [35] G. Erker, *Acc. Chem. Res.* **2001**, *34*, 309.

Received: December 23, 2004

Revised: June 4, 2005

Published online: August 5, 2005